BRNO UNIVERSITY OF TECHNOLOGY
VYSOKÉ UČENÍ TECHNICKÉ V BRNĚ

FACULTY OF CHEMISTRY
FAKULTA CHEMICKÁ

INSTITUTE OF PHYSICAL AND APPLIED CHEMISTRY
ÚSTAV FYZIKÁLNÍ A SPOTŘEBNÍ CHEMIE

TAILORING OF PHASE COMPOSITION AND MICROSTRUCTURE OF CALCIUM PHOSPHATE SCAFFOLDS APPLIED IN REGENERATIVE MEDICINE.

PŘIZPŮSOBENÍ FÁZOVÉHO SLOŽENÍ A MIKROSTRUKTURY VÁPENATÝCH FOSFOREČNANŮ APLIKOVANÝCH V REGENERATIVNÍ MEDICÍNĚ

MASTER'S THESIS
DIPLOMOVÁ PRÁCE

AUTHOR — **Bc. Lucie Pejchalová**
AUTOR PRÁCE

SUPERVISOR — **doc. Ing. David Salamon, Ph.D.**
VEDOUCÍ PRÁCE

BRNO 2020

BRNO UNIVERSITY OF TECHNOLOGY
FACULTY OF CHEMISTRY

Specification Master's Thesis

Project no.:	FCH-DIP1407/2019	Academic year:	2019/20
Department:	Institute of Physical and Applied Chemistry		
Student:	**Bc. Lucie Pejchalová**		
Study programme:	Chemistry for Medical Applications		
Study branch:	Chemistry for Medical Applications		
Head of thesis:	**doc. Ing. David Salamon, Ph.D.**		

Title of Master's Thesis:

Tailoring of phase composition and microstructure of calcium phosphate scaffolds applied in regenerative medicine.

Master's Thesis:

1. Literature review – application of calcium phosphate–based ceramic materials in regenerative medicine.
2. Preparation of calcium phosphate–based ceramic materials by conventional shaping techniques and by freeze–casting.
3. Analysis and evaluation of the influence of the shaping methods on phase composition and microstructure.

Deadline for Master's Thesis delivery: 29.5.2020:

Master's Thesis should be submitted to the institute's secretariat in a number of copies as set by the dean This specification is part of Master's Thesis

Bc. Lucie Pejchalová Student	doc. Ing. David Salamon, Ph.D. Head of thesis	prof. Ing. Miloslav Pekař, CSc. Head of department
In Brno dated 31.1.2020		prof. Ing. Martin Weiter, Ph.D. Dean

ABSTRAKT

Vápenaté fosforečnany jsou nejčastěji využívané keramické materiály v medicíně pro regeneraci kostní tkáně. Vápenaté fosforečnany jsou biokompatibilní, bioaktivní a mezi sebou se odlišují především rozpustností a související degradací v organismu, proto jsou nejčastěji využívány k regeneraci malých defektů nebo jako vrstvy na kovových implantátech. U již zmíněné rozpustnosti materiálu po implantaci, hraje důležitou roli poměr zastoupení jednotlivých vápenatých fosforečnanů, od kterého se pak odvíjí rychlost degradace materiálu v organismu.

Tato práce se zabývá vlivem tvarovacích metod na mikrostrukturu a zejména fázové složení vápenatých fosforečnanů. Výchozím materiálem pro pozorování změn ve fázovém složení byl komerční hydroxyapatit, který byl upraven kalcinací při 800 °C po dobu jedné hodiny. Při kalcinaci došlo k vytvoření dvoufázové směsi, obsahující hydroxyapatit a β-fosforečnan vápenatý. Tato dvoufázová směs byla poté využita pro přípravu suspenze s plněním 15 obj.%, a také k přímé přípravě polotovarů s různou výslednou mikrostrukturou a fázovým složením. S cílem zjistit vliv procesu byly v této práci porovnány vzorky připravené pomocí metod: freeze-casting, izostatické lisování za studena, uniaxiální lisování a suspenzní odlévání. U polotovarů a slinutých vzorků byla provedena charakterizace mikrostruktury a analýza fázového složení. V práci se potvrdil vliv tvarovací metody na oba stanovené parametry – mikrostrukturu a fázové složení. Nově pak bylo zjištěno, že se zvyšující se hodnotou porozity a velikostí pórů se zvyšuje i zastoupení hydroxyapatitu ve vzorcích. Tento trend byl pozorován u vzorků vykazujících unimodální i bimodální zastoupení velikosti pórů.

Klíčová slova: vápenaté fosforečnany, biokeramika, regenerativní medicína, freeze-casting

ABSTRACT

Calcium phosphates are the most used ceramic materials for bone regeneration. Calcium phosphates are biocompatible, bioactive and differ in solubility and related degradation in organism. Therefore, calcium phosphate materials are used to regenerate bone defects of small size and as coatings for metallic implants. The solubility of the used materials in body environment after implantation is determined by the ratio of individual calcium phosphates and related degradation rates.

This thesis deals with the impact of shaping methods on microstructure and phase composition of calcium phosphates. Commercial hydroxyapatite powder was used as a starting ceramic powder and was treated by calcination at 800 °C for one hour. The biphasic mixture of hydroxyapatite and β-tricalcium phosphate was formed during the calcination and this mixture was used for ceramic suspension preparation, with solid loading of 15 vol%, as well as for green bodies preparation. Samples were prepared using several shaping methods: freeze-casting, cold isostatic pressing, uniaxial pressing, and slip-casting. Characterization of both, green bodies and sintered samples was performed and the impact of used shaping methods on microstructure and phase composition, was confirmed. It was also observed that the hydroxyapatite content is increasing with increasing porosity, and pore size. This trend applies for samples with unimodal pore size distribution as well as for samples with bimodal pore size distribution.

Keywords: calcium phosphates, bioceramics, regenerative medicine, freeze-casting

PEJCHALOVÁ, Lucie. Přizpůsobení fázového složení a mikrostruktury vápenatých fosforečnanů aplikovaných v regenerativní medicíně. Brno, 2020. Dostupné také z: https://www.vutbr.cz/studenti/zav-prace/detail/122609. Diplomová práce. Vysoké učení technické v Brně, Fakulta chemická, Ústav fyzikální a spotřební chemie. Vedoucí práce David Salamon.

ACKNOWLEDGEMENT

Firstly, I would like to thank my supervisor doc. Ing. David Salamon, PhD. for his experienced and scientific supervision, all wise suggestions, and discussions. Next, I would like to thank Ing. Jakub Roleček, PhD. for all his advice, patience and help in the lab. I would also like to thank all my colleagues from the research group of Advanced Ceramic Materials at the Central European Institute of Technology, for all their advice and assistance.

DECLARATION

I declare that the diploma thesis has been worked out by myself and that all the quotations from the used literary sources are accurate and complete. The content of the diploma thesis is the property of the Faculty of Chemistry of Brno University of Technology and all commercial uses are allowed only if approved by both the supervisor and the dean of the Faculty of Chemistry, BUT.

……

Student's signature

TABLE OF CONTENT

1 INTRODUCTION

Tissue engineering is an important part of regenerative medicine. The role of tissue engineering is to create a tissue scaffold or replacement with specific properties. In past decades, scientists were interested in advanced materials which should replicate natural human tissues. Due to the increasing average age of the population, there are increasing diseases and injuries of the musculoskeletal apparatus. Nowadays, advances in technologies and materials are required for orthopaedics, surgery and successful treatment [1]. However, repair of critical-size defects remains a challenge. Selection of suitable material and fabrication method for scaffold (bone replacement), preparation depends on the size of bone defect, as well as the causes of the injury or disease. Bone regeneration is a complex process depending on various materials and conditions. Also, many practical factors must be considered, for example, gender, age, health and nature of the disease or injury. Bone repair process, using biomaterials, has been already investigated in the field of clinical research.

Materials that are exposed to living tissue, after implantation or application, are called biomaterials. These biomaterials used in regenerative medicines include synthetic materials such as metals, synthetic or bio-inspired polymers, ceramics or composites, and naturally occurring materials – autografts (patient's tissue) and allografts (donors' bone), polysaccharides (alginate, hyaluronic acid) or proteins (collagen) [2, 3].

Metal alloys were used for bone implants preparation, especially in the past. Metallic materials have excellent electrical and thermal conductivity, high load-bearing capacity, toughness, and ductility. The use of cobalt (Co) and cobalt-based alloys (CoCrMo), stainless steel, titanium (Ti) and its alloys (Ti6Al4V) is clinically proved, and these materials show sufficient biocompatibility, excellent mechanical strength and corrosion resistance. The main disadvantage of metallic implants is their higher stiffness compared to natural bone, which causes stress shielding and improper bone healing. An elastic module of bone tissue is ranging from 0.02 to 30 GPa. Majority of metallic materials have much higher modulus – 110 GPa for titanium alloys, and 210 GPa for cobalt alloys. The difference in elastic moduli results in different stress distribution and may be one of the reasons for implant failure and inflammation. Another disadvantage of using metals, as material for bone scaffold engineering, is the absence of porosity. However, using modern fabrication processes, such as additive manufacturing, especially selective laser melting or metal-based additive manufacturing, offer structure preparation with controlled shape and size of pores. Also, application of post-processing techniques (surface modification or coating) improve the properties of final scaffold and ensure its successful implantation without a negative immune response. Metals remain a good choice especially for healing severe fractures and joint replacement [2, 5].

Polymers and co-polymers replaced metals in tissue engineering during the past decades. The main reason is, that polymeric scaffolds can better mimic the structure and properties of natural bone. Based on the source, polymers are classified as natural polymers and synthetic polymers, or bioinspired polymers. Naturally occurring polymers, such as collagen, chitosan, alginate, or hyaluronic acid, are often derived from natural sources. Using natural polymers sources, suffer from many disadvantages – antigenicity, microbial contamination, and variability in properties. There are many synthetic or bio-inspired polymers already approved for clinical uses – poly(lactic acid), poly(glycolic acid) and their copolymers, poly(ε-caprolactone) etc. Synthetic polymers are easy to fabricate in high quality and all mentioned compounds have been already classified as resorbable polymers. Using these polymers, as a scaffold or implant, significantly reduce complications during bone reparation and can avoid resurgery for removing the implant, if necessary. During scaffold degradation, the material is transferred to the healing bone, preventing the stress shielding. There are also some disadvantages – low mechanical stability or single-phase composition of the scaffold may not always serve as ideal tissue construct. Therefore, they are used especially, in composite with calcium phosphate ceramics or another polymer [3, 4].

Degradable polymer/ceramic composites offer a new therapeutic concept in bone regeneration. Composite scaffolds link the properties of both – polymers and ceramics. Polymers, used as the matrix of scaffolds, are flexible, biocompatible, non-toxic, biodegradable and easy to fabricate. On the other hand, ceramic materials, used as a solid loading, provide the final scaffold mechanical strength and necessary support during the bone repair process. Use of calcium phosphate ceramics offers building material for bone, especially calcium and phosphate ions, naturally occurring in the inorganic part of bone tissue [6].

Bone grafts have been already used for over the centuries. Using autograft for bone regeneration has been clinically approved, but it is not used so often nowadays. Bone regeneration by autografting is limited by the size of defect – reconstruction of large segments is difficult because of limited patient's bone tissue supply. The most commonly used is the allograft bone. Allografts are obtained by surgery from a donor and have all necessary properties (osteoinductivity, osteoconductivity, biocompatibility, etc.) for bone repair process. The main disadvantage is the possibility of negative immune response and inflammation, because allografts may contain antigenic molecules, which can be a limiting factor for sensitive patients [7].

Ceramic materials are an important source of materials applied in medical engineering. Ceramics, which are in contact with human tissues, are called bioceramics. Bioceramics have been used in the middle of the past century, and recently is commercially available in various forms. The most used bioceramic materials will be more described in the literature review [8].

2 LITERATURE REVIEW

2.1 Ceramic materials used in bone repair

Bioceramic materials is a group of inorganic compounds, used in tissue engineering. The major development of ceramic materials has occurred in the last 50 years, especially in fabrication processes, new shaping methods, sintering and analytical and imaging techniques.

Reactivity of bioceramics is also one of the basic criteria in bone regeneration. Related to primary response of the immune system, is bioceramics classified as bioinert, bioactive and resorbable or biodegradable.

If bioinert material is implanted into the body, it initiates immune reaction which leads to encapsulation of implant, creating fibrous non-adherent insulation, approximately 1 μm thick [8, 9]. A similar reaction occurs after implanting metallic or some polymeric scaffolds or implants. Compounds such as alumina (Al_2O_3), and zirconia (ZrO_2) are bioinert ceramics and they both have been used since 1960's. Clinical application of these oxides is for orthopaedic implants and implant components – knee prosthesis or hip implant. Lately, both materials have been used in dental surgery. However, there is a limitation for zirconia – degradation in an aqueous environment. Degradation is due to the phase transformation, but the mechanism is still the subject of many studies. Nowadays composites alumina/zirconia seem to be a good path to improve stability of scaffolds [9].

Bioactive and resorbable ceramics are very closely linked materials. Living tissue reacts with scaffold in both cases. Surface of bioactive ceramic scaffolds is reactive and forms a bond to the living tissue. Body fluids react with the surface only and forming of an apatite-like layer is induced and present bone tissue cells can form a new bone, tightly bonded to the scaffold. Bioactive materials such as hydroxyapatite, bioactive glasses or their composites are used in bulk form, powders, highly porous scaffolds, or granules, as well as, coatings. These ceramics are proper for the reconstruction of small defects. However, they are brittle, and it is impossible to use them for large defects regeneration, where mechanical properties are one of the primary aspects [8].

Changes in ceramic particle size, porosity, or hydrophilicity can turn bioactive ceramics resorbable or biodegradable. The most used resorbable ceramics are based on calcium phosphates or calcium sulphates. These scaffolds are designed to fulfil specific functionality for a certain time period helping in the self-reparation process of bone tissue, which is very complex and depends on time-controlled releasing of calcium ions from the scaffold. Ideally, these scaffolds should be fully resorbed, after a certain time period [8].

2.2 Calcium phosphate ceramics

Calcium phosphates (CaP) are known as the major inorganic component in approximately 70% of human bones. Synthetic calcium phosphates have been studied for clinical use and represent a modern, low-risk approach in bone regeneration. First studies on calcium phosphates properties were published in 1920s and had shown its biocompatibility and bioactivity. Synthetic CaP belong to the group of ceramic materials, which are used in regenerative medicine since the 1980s as bone fillers. CaP materials seem to be mechanically and chemically suitable for bone reconstruction. The group of CaP includes many compounds varying in the chemical formula, Ca/P ratio, density, solubility values, degradation rate etc., but they have many common properties, such as bioactivity, biocompatibility, and most of them are biodegradable [8, 10].

CaP bioceramics are considered as highly favourable scaffold material, because of their natural present in bones. One of the several factors affecting the scaffold's implantability is biocompatibility. It was found that CaP are biocompatible, because they can be dissolved in body fluids, or they can be present in solid bulk form permanently. CaP are also bioactive, promoting cell adhesion and proliferation of osteoblasts. Bioactivity is closely related to resorption of CaP – solubility of the scaffold in body fluids is a very important characteristic and influences scaffold's behaviour in the body [10]. If CaP scaffold dissolves, it is releasing calcium and phosphates ions. Released ions can affect the proliferation of the osteoblast and new bone formation. Calcium ions play an important role in bone matrix formation and calcification. In bones, phosphorous is mainly presented as phosphate ion (PO_4^{3-}) and has a similar effect on bone formation as well as calcium ions [11]. Two-dimensional phase diagram shows solubility of all CaP compounds (Figure 1) – dicalcium phosphate anhydrous (DCPA), dicalcium phosphate dihydrate (DCPD), octacalcium phosphate (OCP), α-tricalcium phosphate (α-TCP), β-tricalcium phosphate (β-TCP), hydroxyapatite (HA), and tetracalcium phosphate (TTCP) [10, 12].

As is mentioned above, the process of bone healing is very complex and consists of the main three partial processes – osteoinduction, osteoconduction and osseointegration. The osteoinductive and osteoconductive properties of scaffold and implantable materials are very important for bone regeneration. Osteoinduction is a process, where pluripotent cells are stimulated (by inductive agent) to differentiate into osteoblasts. Osteoconduction is a continuous process when new bone grows on scaffold's surface. Osseointegration is a more complex process and is related to bone formation around and in the implant. Directly linked cell adhesion is influenced by scaffold properties – surface roughness, crystallinity, phase composition, hydrophilicity, and porosity [13].

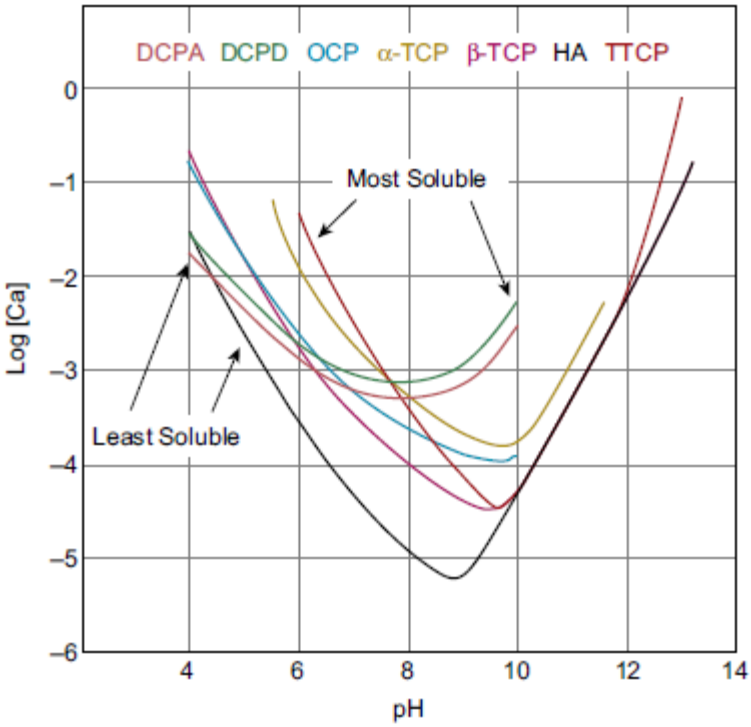

Figure 1: *Solubility phase diagram for CaP compounds [12].*

2.2.1 Hydroxyapatite

Hydroxyapatite (HA) with the chemical formula $Ca_{10}(PO_4)_6OH_2$, and Ca/P ration of 1.67, is a mineral part of teeth and bones and its apatite crystals are naturally occurring in the human body and they are very similar to synthetic HA crystals. Biological HA and synthetic HA differ in stoichiometry (monoclinic, hexagonal), composition, crystallinity, as well as in physical and mechanical properties (Figure 2). HA is the most stable calcium phosphate. Solubility is very low and is affected by temperature, pH, body fluids composition etc. [11].

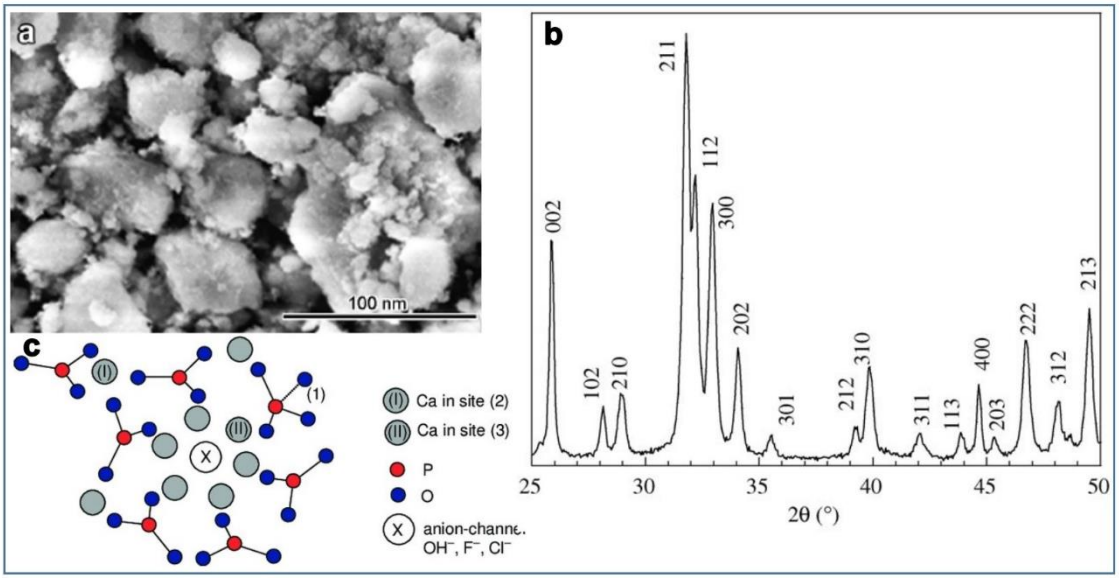

Figure 2: *Chemical and structural characteristics of hydroxyapatite; a – SEM image [14]; b – X-ray diffractometry spectrum [15]; c – schematic illustration of the crystal structure [16].*

Generally, the clinical application of HA is as a bone filler in the form of granules, cements, or pastes, porous scaffolds, and implant coating or drug delivery systems (anticancer drugs). Usage of HA a coating, improves biocompatibility, bioactivity, and biological fixation of metallic implants. Because of its hardness, HA has been used in scaffolds applied in parts with higher mechanical stress. Composites of polymers and HA are also studied for specific properties such as controlled porosity of scaffold, tailored mechanical properties [8, 11, 17].

There are many techniques, how to prepare synthetic HA. Solid-state methods are based on the reaction between raw powders (CaO or $CaHPO_4$). The reaction is basically induced by thermal treatment (temperature exceeding 700 °C) and the final product is well crystallised. Using the mechanochemical method with direct milling of raw materials offers a way for HA nanoparticles fabrication. Wet state methods require low temperatures, but the final product has a lower crystallinity or inaccurate Ca/P ratio. To wet-state methods belong precipitation techniques, which are widely used for their simplicity – mixing two aqueous solutions. other techniques such as sol-gel method, emulsion, or hydrothermal conversion, are also used and provide HA particles with different size, crystallinity, or Ca/P ratio. It is also possible to extract HA from natural sources (fish bones, eggshells, or shrimp shells) [18].

HA is naturally formed and collected in the human body, but its structure can accept many compositional variations in positions of Ca^{2+}, PO_4^{3-} or OH^- groups. Biological HA crystals usually contain other ions such as Na^+, K^+, Mg^{2+}, F^-, CO_3^{2-}, etc. Substitutions in synthetic HA are also possible. Substitutions can help to stabilize the structure; however, they can also change some of the properties (solubility) [9, 17].

2.2.2 Tricalcium phosphate

Tricalcium phosphate (TCP) with chemical formula $Ca_3(PO_4)_2$ and Ca/P ration 1.5 are materials occurring in two phases – α-phase and β-phase. They differ in crystal structure, density, the temperature of formation, or solubility, which determine their biological properties.

Both α-TCP and β-TCP, are currently used in medicine, especially in dentistry, surgery and orthopaedics. Commercial bone cements have α-TCP powder as the major constituent, as well as in a form of granules. β-TCP is the most used material for biodegradable bioceramics. It is possible to use the β-TCP for preparation of dense or highly porous scaffolds, granules and cements. Biphasic ceramics of β-TCP/HA, as well as ceramic/polymer composites, have similar clinical application for bone remodelling [11, 19].

The α-TCP has the monoclinic crystal structure. The structure is less densely packed than β-TCP structure, which leads to a higher dissolution and degradation rate (Figure 3). Proper scaffold resorption in the physiological environment can be tailored by scaffold surface modification, ceramics particle size and size scaffold's surface. The most direct method to synthesize α-TCP is accomplished by thermal treatment of a precursor, for example, β-TCP or

HA. Temperature for the phase transition and α-TCP synthesis is ~ 1130 °C (β-TCP→α-TCP transformation). Temperature between 600–900 °C, is required for α-TCP preparation by solid-state reactions of powders mixture. Higher temperatures are required for hydrothermal preparation. However, in the final product minor amounts of β-TCP or HA can be obtained. Presence of β-TCP phase is related to a partial reversion of already formed α-TCP, caused by very slow cooling rate or long dwell time. Stability of α-TCP can be modified by ionic substitution of calcium or phosphate ions. Partial substitution of calcium ions by Mg^{2+}, Zn^{2+}, or Sr^{2+} ions influences the thermodynamic relation between α-TCP and β-TCP, and its solubility. A similar effect has the phosphate ion substitution for silicate (SiO_4), furthermore several *in vitro* and *in vivo* studies have shown that silicate-doped scaffolds enhance the osteogenic process by releasing silicon ions [19, 20].

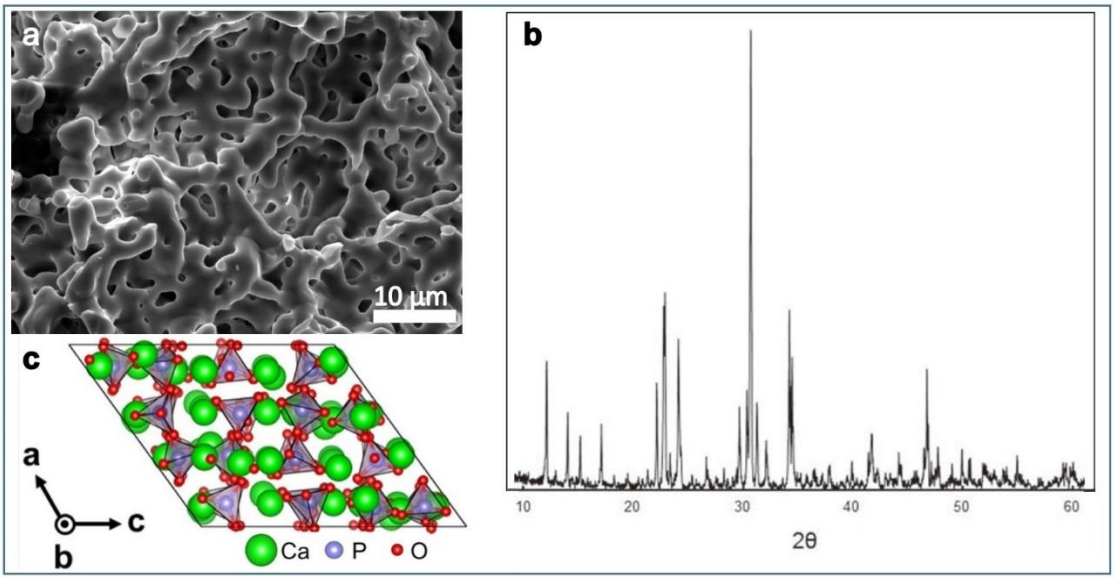

Figure 3: *Chemical and structural characteristics of α-tricalcium phosphate; a – SEM image [21]; b – X-ray diffractometry spectrum [20]; c – schematic illustration of the crystal structure [22].*

β-TCP has the crystal structure of rhombohedral space group. This crystal structure is more stable (more packed), in comparison with α-TCP, so solubility is lower and as well as biodegradation (Figure 4). Despite its lower solubility, β-TCP is still osteoconductive and resorbable. In the past, many *in vitro* and *in vivo* studies had shown that this type of bioceramics is biocompatible and thanks to the chemical and physical properties, also bioactive. Studies had shown that β-TCP implanted into the body is dissolved and replaced by new osteoblasts and bone marrow, depending on scaffold properties, its fabrication way and pH of the physiological environment [19, 23]. Synthetic ways for β-TCP preparation are similar to the α-TCP ones. Pure phase β-TCP is formed, during the solid-state reaction of calcium carbonate and calcium hydrogen phosphate (Equation 1).

$$CaHPO_4 + CaCO_3 \rightarrow Ca_3(PO_4)_2 + CO_2 + H_2O \quad (1)$$

Obtained particles with size around 7–15 μm, can be further modified and sintered [24]. Another option is to use the thermal transition of another calcium phosphate (or their combination), with a transition temperature of 900–1100 °C. Partial ionic substitution is also possible with calcium ions in the β-TCP molecule. Changing the calcium ions for strontium or zinc effects not only stability and solubility but also biological activity. Research of Boanini et al. have shown, that presence of strontium ions in the β-TCP scaffold, have a beneficial action in the osteoporosis treatment. On the other hand, zinc or silver has antibacterial properties, which is an important factor for elimination of post-implant infection [11, 25]. Another option, how to modify β-TCP scaffold properties, is to prepare biphasic ceramic material. Biphasic calcium phosphates, the combination of β-TCP and HA, combine properties of both and possess attractive characteristics, such as different solubility, similar inorganic composition to the bone, bioactivity, and biocompatibility. Studies have shown that β-TCP /HA composites, shaped to the nanoporous or microporous scaffolds, stimulate bone cells differentiation and growth factors, cell adhesion and vascularization etc. Furthermore, the mechanical stability of β-TCP/HA scaffolds is enhanced, which is advantageous for implantation in critical size defects [11, 26].

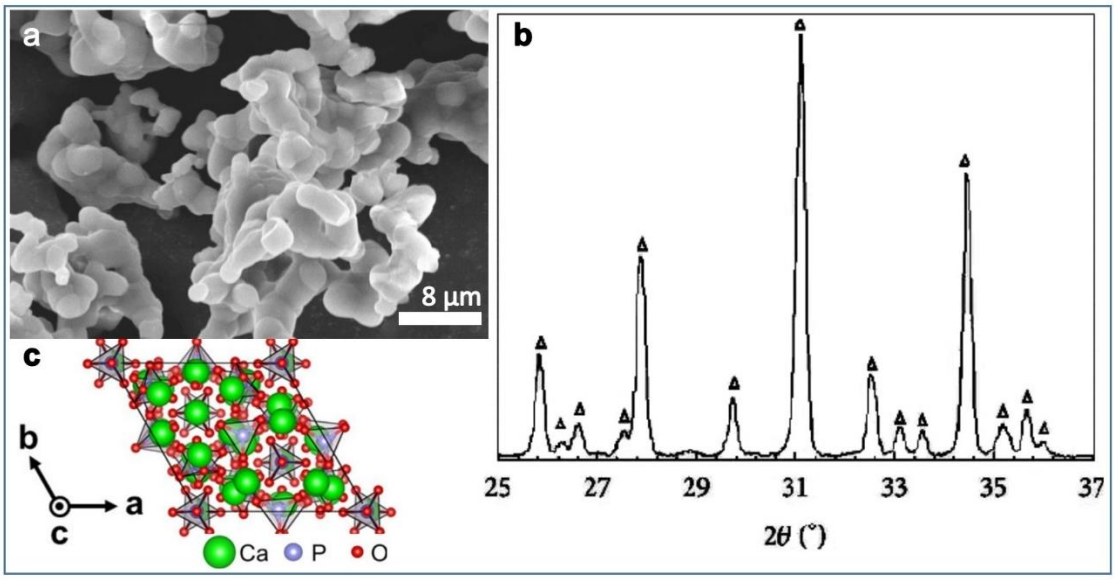

Figure 4: *Chemical and structural characteristics of β-tricalcium phosphate; a – SEM image [25]; b – X-ray diffractometry spectrum [27]; c – schematic illustration of the crystal structure [23].*

2.2.3 Whitlockite

Whitlockite (WH) with the chemical formula $Ca_2Mg(HPO_4)(PO_4)_6$ and Ca/P ration of 1.43, consists of calcium phosphate base, which contains magnesium ion. WH has the crystal structure of rhombohedral space group, as well as β-TCP, but it shows slightly different properties (Figure 5). High stability under acidic conditions and negatively charged surface

causes its higher solubility and the different degradation process, where a higher amount of ions could be released continuously, in comparison with HA [11, 28].

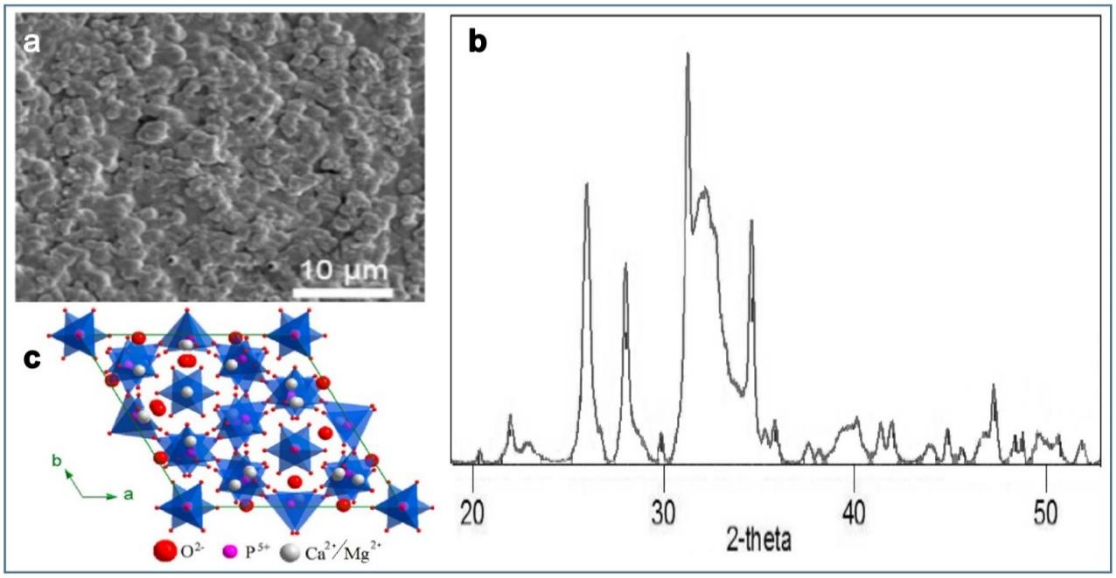

Figure 5: *Chemical and structural characteristics of whitlockite; a – SEM image [29]; b – X-ray diffractometry spectrum [30]; c – schematic illustration of the crystal structure [31].*

Bioactive properties of synthetic WH, have been investigated in *in vitro* and *in vivo* studies, using pellets, powder or polymer/ceramic composites. It has been revealed that the bone remodelling is initiated by increasing ion concentration and protein absorption to WH scaffold surface. Creation of protein-mineral system is a critical factor for bone mineralization, and cellular proliferation [29, 32, 33].

Biological WH is the second most abundant compound in bones, with approximately 20 wt.% of the inorganic portion and is formed in acidic conditions – acidic molecules are produced by osteoclasts, during old bone tissue resorption. The presence of WH increases the compressive strength of bone, as well as bone remodelling.

Synthesis of WH is difficult. However, recent studies have shown that WH can be formed in low-temperature conditions. This reaction is similar to, its biological formation. Acidic conditions (pH < 4.2), and magnesium ions are required in CaP solution. Resulting powder has high purity (without minor phases), and nanoscale particles [11, 33].

2.2.4 Phase transformation of calcium phosphate materials

The phase transition of CaP phases is influenced by presence of metastable phases, amount of water, temperature, Ca/P ratio, and kinetics of CaP system. Hence, it is difficult to describe the solid-state phase diagram precisely. One of the available equilibrium phase diagrams is shown in Figure 6. It has been already described and used by Manjubala et al. for biphasic calcium phosphate (BCP) preparation. Phase diagram also shows the presence of

other several CaP materials, such as dicalcium phosphate (DCPA) or tetracalcium phosphate (TTCP), which are usually used as a minor component in bone cements [34, 35].

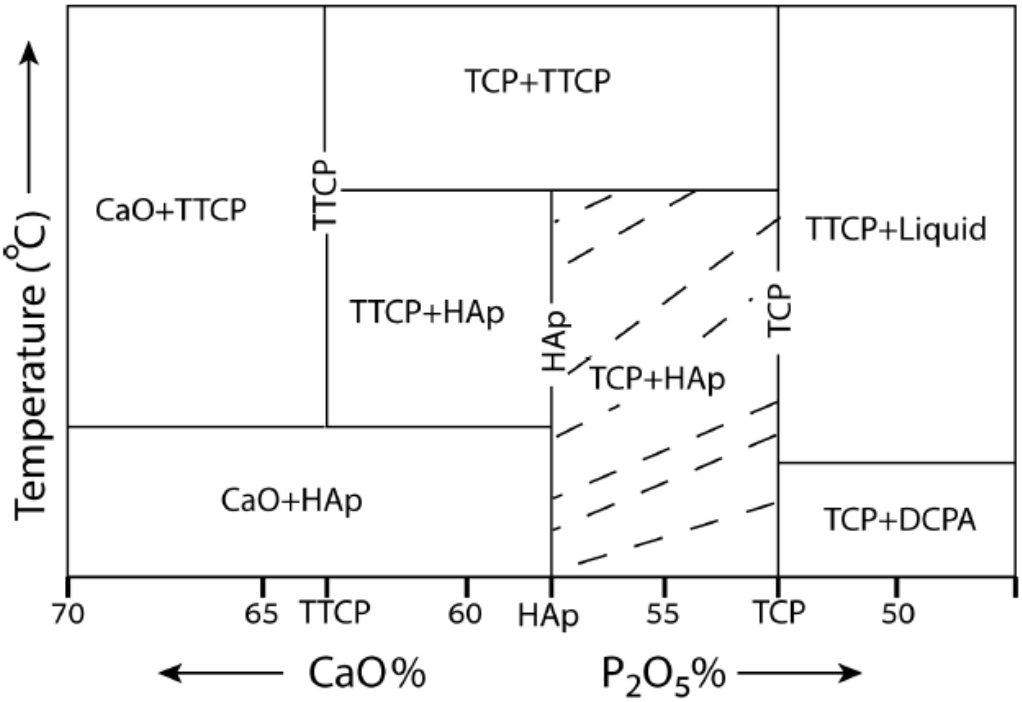

Figure 6: *Solid-state phase diagram of calcium phosphates [35].*

2.3 Classic shaping methods

There are many shaping techniques used for ceramic samples preparation. Powder compacting methods use the pressure to compact free flowing ceramic powder. It is possible to press the powder with or without the addition of a suitable binder. Depending on the final size and shape of samples, the pressure is applied isostatically or uniaxially – isostatic pressing is used for more complex shapes, uniaxial pressing for simple shapes.

Casting methods generally require preparation of ceramic suspension (slurry), where ceramic particles are dispersed in a solvent (usually water) with a small amount of binder. The ceramic suspension is then poured into a mould, which could be porous for removing the liquid by diffusion. Casting methods are shape variable and it is possible to produce both, small and bulk samples.

There are also other methods, such as extrusion, injection moulding or rapid prototyping, used for samples of irregular shape. Some of them are more advanced and complex, as well as samples prepared using these methods.

Using classic shaping methods, the green body is prepared, and it could be further modified or machined to final size and shape. The last step of whole processing is the sintering, where binders and other organic components are burned out and the whole sample is densified and strengthened [9].

2.3.1 Uniaxial pressing

Uniaxial pressing is a compacting method, which applies uniaxial pressure to the powder. Basically, uniaxial pressing includes three steps: filling the die with a controlled amount of ceramic powder, compacting the content, and ejecting the pressed green body (Figure 7).

Preferred particle size distribution is 20–200 μm because a high-volume fraction of small particles causes problems with particle flow, which can lead to the irregular density of the green body. According to the used material, and application of resulting structure, the pressure can be up to 300 MPa [9, 36].

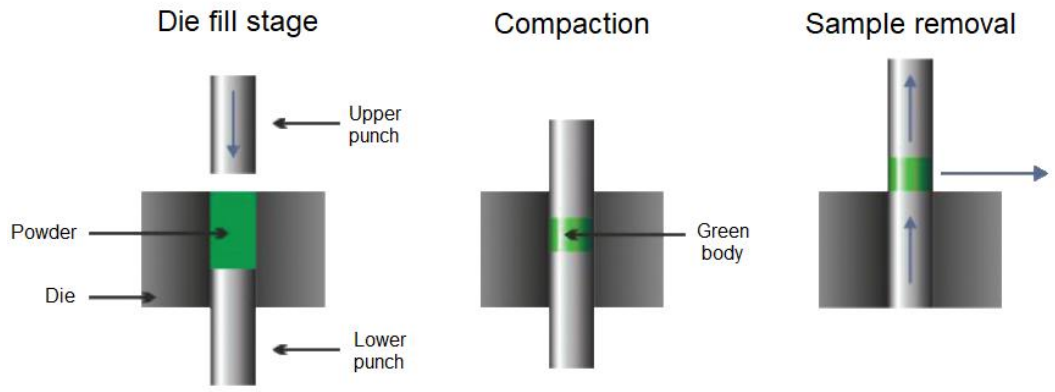

Figure 7: *The stages in uniaxial pressing [36].*

Uniaxial pressing is suited to the simple solid shapes of samples, of any size – large components and small flat parts. Because uniaxial pressing is technically simple, quick, and inexpensive method, it is the most used fabrication process for high-volume ceramics in the industry [9].

2.3.2 Cold isostatic pressing

Cold isostatic pressing (CIP) is another method based on ceramic powder compaction and is conducted at room temperature. CIP applies pressure from multiple directions through a liquid medium (usually special oil, or a mixture of oil and water), which is all around the sample. The wet-bag CIP process includes three steps: the amount of ceramic powder is weighed into a rubber (generally flexible) bag or mould. Mould is sealed and placed inside a high-pressure chamber, which is filled with fluid (Figure 8). Finally, the powder is hydrostatically pressed. After pressing, the pressure is released slowly, and the sample is removed from the mould or bag. It is also possible to pre-shape samples for CIP using uniaxial pressing.

Used pressures range from about 20 MPa up to 1 GPa, depending on the material and its further application. Using the wet-bag process offers samples with a wide range of shapes and sizes, and uniform density, however control of shape and dimensions is poor, and samples

may have to be further processed. This type of process is better for laboratory use, because of long cycle times [9].

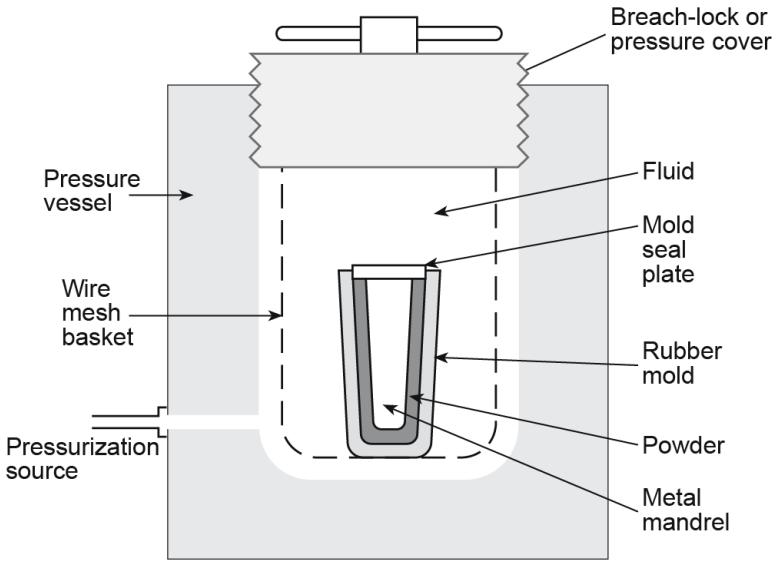

Figure 8: *Schematic illustration of a wet-bag cold isostatic pressing [9].*

Properties of both, green bodies and final samples obtained by CIP, are influenced by applied pressure during the compaction. A high density of the green body leads to the high density of the final sample. In fact, CIP acts like a pre-sintering, and causes particle packing and reorganizing, which normally takes place in the first stage of sintering [37]. Hence, used sintering temperature could be decreased, for the same sample's final density. Also, the volume of the open pores decreased with applied pressure, which improves mechanical strength and fracture toughness [38, 39].

2.3.3 Slip casting

Slip casting is simple shaping method carried out at room temperature. Preparation of ceramic suspension is required, and the quality of suspension affects the final quality of the sample. Consequently, it is necessary to provide proper viscosity of suspension with homogenously dispersed ceramic particles. When the slurry is poured into the mould, water is sucked out by the capillary forces. After drying and sintering, final product with the desired size and shape is obtained [9, 40].

Slip casting is a standard method for fabrication of technical, advanced, and structural ceramic components. However, this shaping method has some limitations, when details are cast. Detailed parts can be damaged upon separation from the mould, especially when the shaped parts are in the uncured state very delicate [9, 41].

2.4 Freeze-casting

Freeze-casting, also known as ice templating, is advanced shaping method, used for porous structures fabrication. Over the past 20 years, freeze-casting has been applied to several materials, but nowadays ceramic or polymeric materials are the most used. In 2001, Fukasawa et al. [42] reported that porous alumina ceramic with complex pore structure can be obtained by freeze-casting method. Since then, this technique has been further developed and described. Moreover, freeze-casting still shows its variability in materials and solvents, which can be used for porous structure fabrication.

The freeze-casting process involves suspension, consisting of a liquid solvent (usually water) and solid phase. During the solidification, solvent acts as a pore forming agent and the solid particles are pushed aside from the moving freezing front. The solubility of solid phase in solvent must be very low, only then the segregation during freezing is ensured. Freezing or solidification step is followed by sublimation of the solidified solvent. The pores that are the replica of the solvent crystals is finally obtained at the first step. Generally, a complex process like freeze-casting can be influenced by many processing parameters, mostly by the composition of ceramic suspension, and freezing conditions [43].

The whole processing of ceramics freeze-casting can be divided into four steps (Figure 9). In the first step, ceramic suspension is prepared. Then, the ceramic suspension is controlled solidify and the porous structure is formed. The solidified solvent is removed during the lyophilisation and pores are revealed. Finally, green bodies are densified during the sintering process [44, 45].

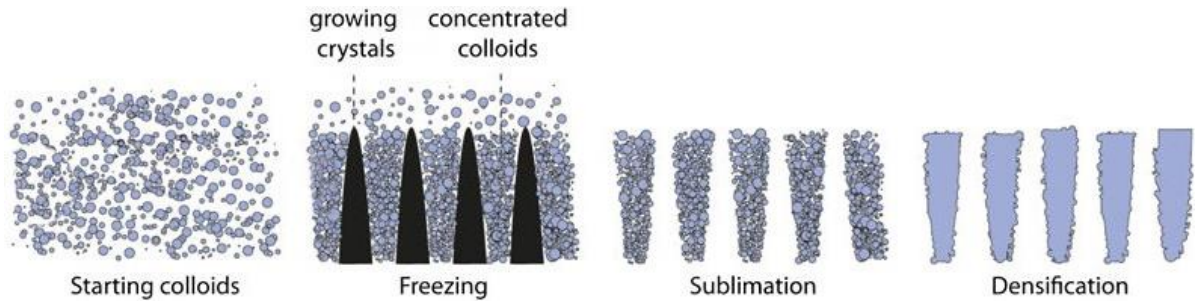

Figure 9: *Schematic illustration of freeze-casting process [45].*

Basically, freeze-casting can be used for preparation of technical ceramics and bioceramics, or composites structures. Depending on used solvents and additives an architecture of porosity can be of any nature – dendritic, lamellar, cellular etc., directional or unidirectional, as well as pore sizes (from nano- to macroscale). Resulting porosity can reach values up to 90 % [44, 46].

2.4.1 Materials and solvents

As is mentioned above, freeze-casting can be applied to a wide variety of materials. However, the most used are ceramic materials. Many papers were already published for using alumina, zirconia, silicate ceramics, hydroxyapatite, TCP ceramics, bioglass etc., as a solid phase in ceramic suspension. Several conditions must be met for using of ceramic materials – sufficient dispersibility of ceramic particles in a solvent, low sedimentation rate and absence of chemical reactivity [46].

A variety of solvents can be used for the preparation of freeze-casting suspension – water, camphene, tert-butyl alcohol, or any organic solvent with an acceptable melting point. Mentioned solvents differ in physical properties (Table 1) and working conditions correspond to the temperature range, where the used solvent is in the liquid phase. In the case of water, room temperature is required, but for camphene-based suspensions, the temperature is 60 °C, and for tert-butyl alcohol 8 °C [47].

Table 1: *Physical properties of solvents used for freeze-casting [47].*

Chemical	Density [g/cm^3]	Boiling temperature [°C]	Freezing temperature [°C]	Surface tension [mN/m]
Water	1.00	100	0.0	73.1
Camphene	0.84	155	44.9	sublimes
Tert-butyl alcohol	0.78	82.5	25.3	20.7

Resulting pores obtained by solidification of water, are of lamellar nature. Dendritic pores can be obtained by using camphene, and in the case of tert-butyl alcohol are pores of prismatic nature [47]. Depending on freezing conditions and solid loading of used suspension, pore size ranges from 4 μm to almost 500 μm. Comparison of resulting structures and ranges of pore size, generated by using different solvents is shown in Figure 10 [46].

Camphene ($C_{10}H_{16}$) is naturally occurring bicyclic monoterpene. It is safe and inexpensive solvent with a melting point about 45 °C. At the room temperature is camphene crystalline, and large gradient of camphene vapour pressure exists between the crystals surface and surrounding atmosphere, which is advantageous because camphene can be sublimated without the assistance of a vacuum pump. During freeze-casting, dendrites of camphene grown in specific crystallographic directions. This freezing behaviour results in the formation of interconnected bicontinuous structure. Camphene-based suspension negatively changes its volume during solidification (-3.1 %). Camphene-based ceramic suspensions can be used very dilute, with very low solid loadings, so it is possible to prepare highly porous structures with interconnected pore channels [44, 47, 48].

Tert-butyl alcohol (TBA) is an organic solvent, which allows flexible freezing and obtained pores have the structure of long straight prisms without branches. TBA can be removed from the solidified structure by rapid volatilization at 80 °C, which is a much faster process than standard lyophilisation Using TBA-based suspension is also usually used for unidirectional freezing, with unidirectionally oriented pores are obtained. Structures with specific pores can be also obtained by using suspension with solid loading around 10 vol.% [47, 49].

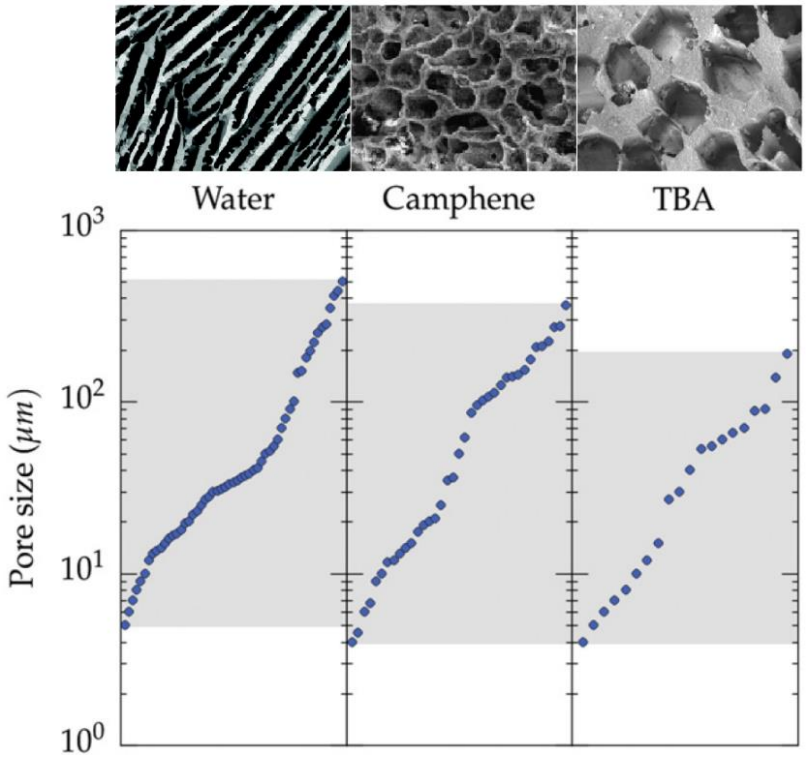

Figure 10: *Porous structures and range of pore size achieved by using different solvents [46].*

The most commonly used solvent is water, due to its unique properties, economic and environmental aspect. Another advantage is the simplicity of processing or using functional additives. Pores obtained by freezing of the water-based ceramic suspension, have lamellar structure. The surface of lamellae usually exhibits some roughness, because of the dendritic morphology of ice crystals. Lamellae can be connected with interlamellar bridges [43, 46]. However, resulting lamellar structure can be influenced by using cryoprotectants or any additive, which are added in the suspension. The effect of additives on the resulting structure will be described down below. During the freezing, water positively changes its volume (+9 %), so as well as in the case of camphene, used mould should be customized. The water expansion induces a phenomenon called freeze-pressing Its effect on ceramic particles has already been described by Zheng et al [50]. The disadvantageous is, that water has low vapour pressure and freeze-dryer must be used for water sublimation [44].

2.4.2 Ceramic suspensions for freeze-casting

Several components are required for ceramic suspension preparation – solvent, ceramic particles, and processing additives, such as dispersant or binder. The solvent is a liquid medium, where ceramic powder must be dispersed. Optimal range of particle size is 0.5–2 μm [46, 51].

For controlling the dispersion and its stability, the dispersant is often used. Using the dispersant reduces particle agglomeration and flocculation. Agglomeration and flocculation change properties of suspension, which usually lead to an inhomogeneous structure of the final sample.

Presence of binder is also required, for increasing the strength of the green body, after sublimation. Absence of organic binder (polyvinyl alcohol, methylcellulose, polyvinyl butyral, polyethylene glycol, etc.), causes a collapse of the green body [43, 44, 51].

The main advantage of water-based ceramic suspension is, that many water-soluble additives can be used to influence the suspension properties or its behaviour during the freezing. Gelatine can be used to affect suspension's rheological properties, changes in phase diagram and corresponding changes in freezing behaviour can be induced by NaCl, reduction of pH (using the citric acid) is affecting the interparticle forces. Using the cryoprotectants, such as sucrose, glycerol or ethanol affects ice growth kinetics and resulting structure [52, 53].

2.4.3 Freezing process

Freezing process can be realized in two different ways – unidirectionally and from multiple directions. Unidirectional freezing is the most used, and normally the direction of freezing is from bottom to up. Scaffolds obtained by unidirectional freezing have a well-organized structure with desired pore size. Several setups can be used for freezing – cooling plate with a temperature gradient, freezing or cold bath (liquid nitrogen, ethanol) with fixed temperature, etc. Four conditions must be satisfied to obtain porous ceramic samples – particle trapping and particle rejection, and suitable properties of ice front (morphology and freezing velocity) [44].

Interactions between solidification front and ceramic particles

During freezing, ceramic particles must be rejected from the advancing freezing front and entrapped between the forming ice crystals (to create pores). The interaction between the freezing front of the solvent and the ceramic particles in suspension must be considered to understand the physicochemical aspect. Together with solidification front velocity, the interaction determines rejecting or engulfing of ceramic particle. To this approach, a simple thermodynamic criterion can be used – changes in surface energy. To achieve this condition, repulsive force and attractive force must be in balance. Repulsive force sustains the ceramic

particle in the liquid phase of the solvent. On the other hand, attractive force pushes the particle against the solidified phase of the solvent. For particle rejection by freezing front, overall surface energy must Δσ be positive

$$\Delta\sigma_0 = \sigma_{ps} - (\sigma_{pl} + \sigma_{sl}) > 0\,, \tag{2}$$

where $\sigma_{ps,}$ σ_{pl} and σ_{sl} are interfacial surface energies associated with the particle-solid ($\sigma_{ps,}$), particle-liquid (σ_{pl}), and solid-liquid (σ_{sl}) interfaces. If the criterion of interactions is not satisfied, the ceramic particle is engulfed by freezing front.

Morphology of the freezing front is a very important condition for successful preparations of porous scaffolds. If the freezing front is planar, rejected ceramic particles are collected only on one side of the sample. Sufficient redistribution of ceramic particles, where the rejected particles are trapped between the arms of the freezing front, must be ensured for successful pores creation. Morphology of freezing front then determines the pore structure in resulting sample.

Solidification front velocity has a significant effect on the size of interlamellar spacing and thickness of lamellae in water-based ceramic suspension. It was shown, that size of interlamellar space λ decrease, as the freezing front velocity increases. Recently, Deville et al. has shown the effect of freezing front on the lamellae thickness, using alumina suspension (Figure 11) [44, 51].

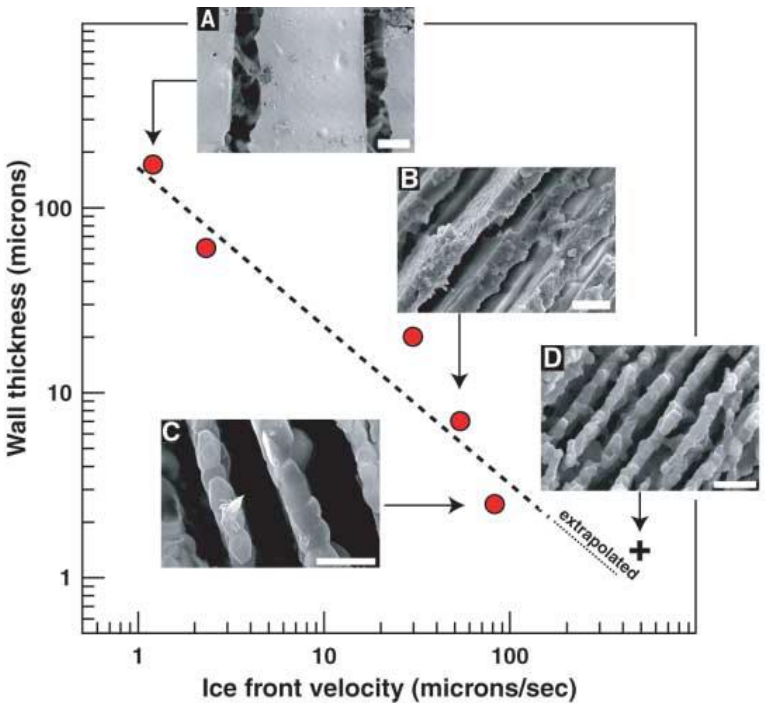

Figure 11: *Dependence of wall thickness on freezing front velocity, using alumina suspension [54].*

Stages of directional freezing

There are three stages of directional freezing – initial, transition and lamellar growth. At the very beginning of directional solidification, the nucleation of ice crystals occurs, and planar freezing front is formed. Because of very high velocity (approximately 750 μm/s), there is no time for particle redistribution, and particles are engulfed by the freezing front. The structure of the initial zone is the result of anisotropic distribution of ceramic particles [44, 55].

The initial freezing front then undergoes the transition to some regular morphology. Solidification slows down, in the second stage of freezing, and the cellular interface of the solidification front is formed. Ice is formed in two different crystal groups – lamellar and pseudolamellar and the resulting structure of the transition zone is a combination of several types of pores.

In the final stage, where freezing front velocity is steady (between 10–100 μm/s), state lamellar growth is obtained. In the case of water-based ceramic suspension, the lamellar structure is created in this zone. The thickness of lamellae is a result of chosen freezing velocity, as well as the size of interlamellar spaces. [44, 54, 55]

2.4.4 Freeze-drying

After freezing, the solidified solvent is removed from the scaffold by lyophilization (freeze-drying). It is a slow two-step process, normally used in the food industry, pharmaceutics, biochemistry, or biology. It takes 24–48 hours to sublimate the ice depending on the size of the sample. It has not been found that the lyophilisation can affect resulting microstructure.

Process of lyophilisation can be divided into two stages – primary drying, and secondary drying. During the first stage, ice is sublimed from the scaffold. Water vapours pass through the dried parts of the scaffold into its surface and are transferred from the vacuum chamber to a cold trap, where the ice is formed again. In this stage, created pores are revealed, and they are the replica of sublimed ice crystals. Secondary drying includes the removal of residual water from the green body [56, 57].

2.4.5 Resulting structure and properties

Structure and pores

Samples prepared by freeze-casting of water-based ceramic suspension can be divided according to the microstructure, into three zones (Figure 12). Zone 1 corresponds to the initial stage of freezing, and no porosity can be obtained. In zone 2, pores with cellular morphology are present. Finally, desired lamellae can be seen in zone 3, where pores run from the bottom to the top.

Samples with lamellar structure consist of ceramic walls and pores – interlamellar spaces. The ceramic walls usually exhibit roughness, because of dendrites created during water freezing. Ceramic bridges can be also observed between walls of adjacent lamellae.

Porosity achieved by freeze-casting ranges between 30–85 %, which depends on the solid loading of the initial suspension. Lower solid loading provides the higher formation of macropores, however, it decreases the mechanical stability of the resulting sample. Total porosity can be also affected by the presence of additives and particle size distribution [43, 54].

As it is mentioned above, the size of interlamellar spacing and lamellae thickness can be tailored by increasing or decreasing the freezing front velocity. Usually, the interlamellar spaces range between 20 and 200 μm. Smaller interlamellar spacing can be achieved by higher freezing rate. It is possible to prepare very thin ceramic walls – approximately 5 μm, but only by applying a fast cooling rate [54].

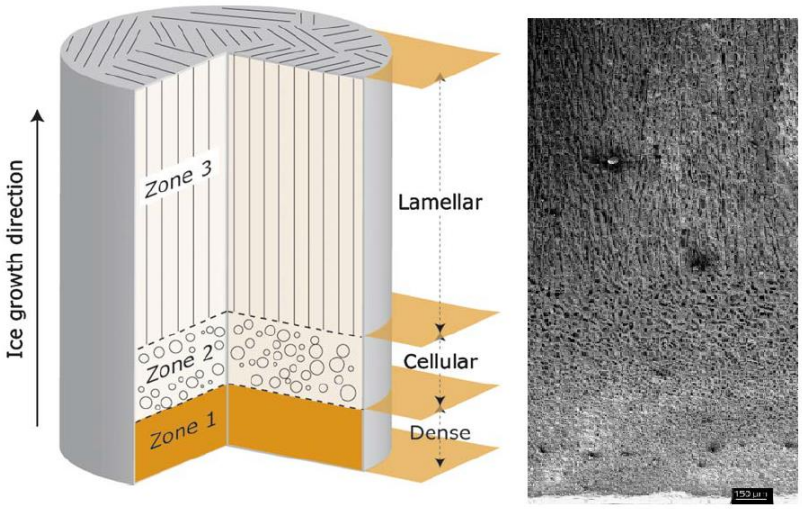

Figure 12: *Typical sample's structure with three distinctive zones [58].*

Using additives for controlling the structure

Changes in the freezing kinetics, solidification, final structure, or properties of the resulting scaffold can be induced by using additives. For water-based ceramic suspension, nearly any water-soluble compound can be used and increase the versatility of processing [43, 52].

Additives used for cryopreservation (cryoprotectants) shifts the solidifying point to lower temperatures. A proper amount of glycerol, added to the aqueous suspension, shifts solidifying temperature from -1.6 °C to -9.6 °C, and decreases volumetric expansion of water. Glycerol also affects the resulting structure of freeze-casted ceramics – pores evolve from lamellar to small dendritic ones and an increase of ceramic bridges can also be observed [59]. Other several anti-freezing agents such as sucrose, or sodium chloride modify roughness of ceramic walls and density of ceramic bridges between adjacent walls [52].

Effect on resulting ceramic structure with using the several other additives, such as polyvinyl alcohol and polyethylene glycol, has been already reported by Li et al. and Zuo et al. [59, 60].

Mechanical properties

The most important mechanical property of freeze-cast scaffold is compressive strength. Samples with lamellar structure show significantly higher values of compressive strength, compared to samples with cellular pores. Despite the high porosity (more than 60 %), the strength values reach more than 15 MPa. Figure 13 shows, that if the porosity decreases, compressive strength rapidly increases. With the value of 145 MPa at a porosity of 47 %, the freeze-cast scaffold reaches the strength comparable to compact bone. For HA scaffolds it is a great improvement, considering their application as the bone replacements.

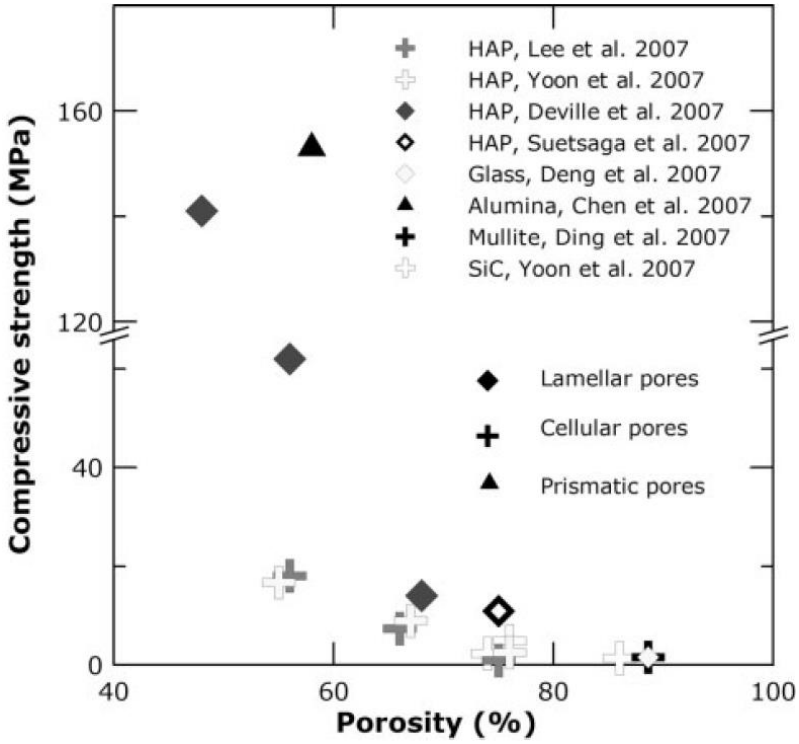

Figure 13: *Dependence of compressive strength on porosity, considering pore morphology and used materials [44].*

Generally, compressive strength depends on several parameters – a type of ceramic material, particle size and shape, pore morphology, size and dimensions, and homogeneity of the structure.

Compressive strength of freeze-cast ceramics can be modified by different cooling rates. As the cooling rate increases, the strength also increases. The explanation corresponds to the pore size – as the freezing rate increases, the pores become smaller, and the whole structure is mechanically more stable [43, 44].

3 AIMS OF THE THESIS

1. Literature review – application of calcium phosphate-based ceramic materials in regenerative medicine.
2. Preparation of calcium phosphate-based ceramic materials by conventional shaping techniques and by freeze-casting.
3. Analysis and evaluation of the influence of the shaping methods on phase composition and microstructure.

4 MATERIALS AND METHODS

The preparation of CaP scaffolds, using freeze-casting and classic shaping methods, such as slip-casting, uniaxial pressing or cold isostatic pressing, entailed many steps, which will be described in this part of the thesis, as well as instruments used for processing and characterization.

All ceramic samples were produced, using the commercial hydroxyapatite powder (Sigma Aldrich).

4.1 Processing

The porous ceramic scaffolds were prepared by controlled freezing of ceramic suspension. The same ceramic suspension was used for dense samples, prepared by slip casting. For the preparation of dense samples prepared by uniaxial pressing and cold isostatic pressing calcined hydroxyapatite powder was used.

4.1.1 Powder treatment

Commercial hydroxyapatite (purum p.a., >90 %, Sigma-Aldrich) was used as a starting ceramic material in this research. Before further use, the hydroxyapatite powder was calcined at 800 °C per 1 hour, in air. During the calcination present carbonates are removed and ceramic powder coarsens, due to grain growth.

4.1.2 Freeze-casting suspension

Ceramic suspension used in this research was prepared four main components. First, water-based solution of poly(vinyl alcohol) – PVA (Mowiol® 10-98, M_W ~ 61.00, Sigma Aldrich). PVA was used as an organic binder. The second component was a dispersant – Dolapix CE64, which was used for a continuous distribution of ceramic particles in the suspension and their stabilization. Sucrose was used as a freeze-casting additive, which improves the mechanical stability of green bodies, and the creation of interlamellar bridges. Ceramic powder – calcined hydroxyapatite, was used as solid loading of suspension. Finally, a small amount of octanol helped to decrease surface tension and to eliminate air bubbles in the suspension.

Firstly, the PVA solution was prepared. To the amount of 1000 ml of distilled water 9.61 g of PVA crystals were added and placed into the water bath at a temperature of 97 °C, with constant stirring at 250 rpm, until complete dissolution of the crystals. After cooling down, a given amount of PVA solution was weighed into a plastic bottle, with a proper amount of zirconia milling balls. Sucrose, dispersant, calcined hydroxyapatite, and octanol were gradually added to the solution. The suspension was then placed on a roller mixer for at least 24 hours.

Hydroxyapatite suspension was made in one variant only (ICE-15 % HAP+S). The exact composition of used suspension is shown in Table 2.

Table 2: *Hydroxyapatite suspension ICE-15 % HAP+S.*

Chemical	Density [g/cm^3]	Weight [g]	Weight %	Volume %
Water	1.00	51.55	59.32	79.11
Poly(vinyl alcohol)	1.19	1.05	1.21	1.39
Sucrose	1.52	2.30	2.65	2.18
Dolapix CE64	1.20	2.00	2.30	2.32
Hydroxyapatite	3.13	30.00	34.52	15.00
Octanol	0.83	0.06	-	-

4.1.3 Freeze-casting

In this research, three types of freezing were used to achieve different porosity and phase composition. Various types of freezing rates were performed by using the cooling plate, freezing bath with liquid nitrogen, and dipping in Dewar flask with liquid nitrogen, see Table 3. Our freeze-casting apparatus with a freeze dryer is shown in Figure 14.

Table 3: *Freezing front velocity assigned to the type of freezing.*

Type of freezing	Sample identifier	Freezing front velocity [μm/s]
Cooling plate	I-T 50	3.4 ±0.3
	I-T 20	5.5 ±0.2
Liquid nitrogen (freezing bath)	V1	12.7 ±0.5
	V2	25.8 ±1.2
Liquid nitrogen (Dewar flask)	V3	~ 1000

Two types of drying were applied for each type of freeze-cast samples after the freezing step. Freeze-drying was applied at low pressure and room temperature, overnight (LYO is added to the sample identifier). To investigate the effect of sublimation, if there is any, comparative sets of samples were air-dried (AIR is added to the sample identifier). Freeze-cast samples were placed into the weighing dish, where the samples were thawed (cast) and dried overnight on air. On the second day, air-dry samples were placed in the dryer for 45 minutes, at 40 °C.

Figure 14: *Freeze-casting apparatus.*

Freeze-casting with the controlled temperature gradient

Freezing of ceramic suspension with a controlled temperature gradient was performed by using the cooling plate (Medite). After removing the bubbles, the suspension was poured into a poly(lactic acid) – PLA mould with a copper block in the bottom and the inner diameter of 24.5 mm. The mould was pre-cooled, as well as the cooling plate at -5 °C. The process of freezing usually takes two and half hour. After complete freezing, scaffolds were quickly removed from the mould and placed in a freezer before further processing.

Two types of cooling rates were used – faster freezing with temperature gradient - 5 °C/20 min (I-T 20), and slower with temperature -5 °C/50 min (I-T 50).

Freeze-casting with liquid nitrogen

Rapid freezing of ceramic suspension was performed in three different ways. In this case, only one sample was prepared in one freezing cycle. The used mould was the same as in the case of freezing with the cooling plate.

For the slowest version (Version 1 – V1), freezing setup consisted of four parts. Insulating polystyrene underlay, used as a prevention of the heat transfer from the surroundings to the mould, plastic dish, where the liquid nitrogen was poured, aluminium ring and aluminium plate. The ceramic suspension was poured into a pre-cooled mould and the mould was placed on the aluminium plate, pre-cooled by liquid nitrogen. Liquid nitrogen was continuously added into the plastic dish during freezing. Simultaneously, the time of the freezing process was measured.

The similar set up was also used for the faster version (Version 2 – V2). The only difference was the omission of the aluminium ring, so the aluminium plate was placed directly into the plastic dish with liquid nitrogen. Pre-cooled mould with ceramic suspension was placed directly into the freezing bath. The time of complete freezing was also measured. Scaffolds were quickly removed from the mould and placed into the freezer after freezing.

The fastest freezing was carried out by dipping a mould with suspension in a Dewar flask filled with nitrogen (Version 3 – V3). As a mould was used a plastic Pasteur pipette, in this case. A piece of string was attached to the filled pipette, and the whole set was dipped in liquid nitrogen. After 10 seconds, the frozen mould was pulled out. Samples were quickly removed from the pipette and placed into the freezer.

4.1.4 Slip casting

The slip casting process was performed using the same ceramic suspension as for the freeze-casting (ICE-15 % HAP+S). A given amount of mixed and deaerated suspension was poured into a weighing dish, where the suspension was air-dried overnight. Next day, the air-dried suspension was placed in a dryer for 45 minutes, at 40 °C.

4.1.5 Uniaxial pressing

The uniaxial pressing of ceramic powders requires the use of two punches and die. The used pressing set was consisted of two stainless steel punches and a stainless-steel die with 16 mm inner diameter. The process of uniaxial pressing the pellets includes few steps. Firstly, both the die and the punches were cleaned and coated with a solution of PVA in ethanol. Then, approximately 0.5 g of calcined hydroxyapatite powder was poured into the die. The whole set was placed in the hydraulic press (Brio Hranice, BSML 21 – MT 20) and pressed at 10 MPa.

4.1.6 Cold isostatic pressing

For isostatically pressed pellets preparation, uniaxially pressed pellets were used. Green pellets were inserted into an elastic cover (a medical probe cover), keeping a certain distance. Inner space of the elastic cover was evacuated and sealed. Set of pellets was placed in the isostatic press apparatus (P/O/ WEBER Laborpresstechnik, KIP 300 E) and isostatically pressed at 250 MPa – for the first set of samples, and at 700 MPa for the second set. After pressing the whole assembly was removed from the press, the elastic cover was cut, and pellets were taken out carefully.

4.1.7 Sintering

After shaping processes, samples were placed on the alumina plate and sintered in laboratory furnace (CLASIC HT1200M). All samples were sintered at 1200 °C in the air for

120 minutes. The heating rate was set on 2 °C/min up to 600 °C, and 5 °C/min up to 1200 °C. The cooling rate was set on 5 °C/min down to 700 °C. Then, cooling was spontaneous.

4.2 Characterization

Characterization of green bodies and sintered freeze-cast, slip-cast, and pressed samples was performed to compare the microstructure, porosity and phase compositions changes. Following analytical methods were used in order to characterize prepared samples: scanning electron microscopy, optical microscopy, density measurement, mercury porosimetry, Raman spectroscopy and X-ray diffractometry.

4.2.1 Scanning electron microscopy

Images were taken using the High-Resolution Scanning Electron Microscope (FEI Verios 460L). Verios is a field-emission scanning electron microscope, with sub-nanometer resolution and wide energy range. The microscope is equipped with the number of imaging and analytical detectors.

Images are assembled by scanning secondary and backscattered electrons. Secondary electrons images reveal the topography of sample's surface. Backscattered electrons are scanned for compositional contrast creation.

4.2.2 X-ray diffraction

X-ray diffraction (XRD) spectra were taken using the Rigaku SmartLab 3 kW, which is high-resolution diffractometer with Cu anode. The XRD was operated at 40 kV voltage and 30 mA current, in Bragg-Brentano measurement mode. Both, the surface of bulk samples, and a small amount of the ceramic powder from crushed samples were measured by XRD analysis.

No special sample preparation is required for bulk samples, but it is necessary to choose the samples with a smooth surface. Preparation of powder samples is more complicated and must be performed quickly and gently. If it is possible, crushing and grinding must be ensured, in the first step. In the second step, the sifting of ceramic powder can be done. Finally, the ceramic powder is poured on the special glass and the surface is aligned.

Determination of the HA and TCP from XRD spectra were received by using the simple height law for the I_{100} peaks. Percentage of HA was determined by the following formula:

$$\mathrm{HA}\ [\%] = \frac{\mathrm{I}_{100}\ (\mathrm{HA})}{\mathrm{I}_{100}\ (\mathrm{HA}) + \mathrm{I}_{100}\ (\mathrm{TCP})} \cdot 100 \tag{3}$$

4.2.3 Raman spectroscopy

Raman spectra of both, dense and porous samples were taken using the Witec Alpha 300R, which is Raman imaging spectrometer with a lateral resolution of approximately 200 nm. The wavelength of used laser was 532 nm.

Generally, no special sample is required. However, in this research, the dense samples were embedded in polystyrene and porous samples in epoxy resin. Then, samples were polished and Raman spectra were measured as a comparison to the XRD.

4.2.4 Density measurements and porosity determination

The density of the samples was measured using the analytical balance with the kit for density determination (Mettler Toledo, XSE 204). Density measurements were performed using the Archimedes method (EN 623-2 [62]). This method allows, jointly with the knowledge of the material's theoretical density, to determine the ratio of closed and open porosity inside the sample.

The density of each dense sample was measured after sintering. In the first step, removing residual wetness was done. Firstly, the mass of the sample in the air was measured. Then, the sample was placed in a desiccator and desiccator was evacuated. Consequently, distilled water with the addition of a small amount of detergent was infused in the desiccator and the whole sample was submerged. Finally, the apparent mass of the sample was measured, as well as the mass of the sample in the air with open pores filled with water. For relative density calculation, the following formula was used:

$$\rho_{rel} = \frac{m_s \cdot \rho_{H_2O}}{(m_p - m_A) \cdot \rho_{teor}} \cdot 100 \quad (4)$$

The porosity of dense green bodies and sintered porous scaffolds was defined from the sample's weight and dimensions. The calculation was performed using the following formula:

$$\Pi = 1 - \frac{\rho_{scaff}}{\rho_{teor}} \quad (5)$$

4.2.5 Mercury porosimetry

Porosity measurements were performed using the mercury porosimeter Pascal440, Thermo Fisher Scientific, with measuring pressure at 330 MPa.

No special sample preparation is required, the dimensions of the sample must be adjusted to the size of the chamber, however. This method allows to determine pores with size between 0.001 and 100 μm.

5 RESULTS

The prepared samples were divided into three groups, according to the processing and their properties. Short description of each group can be seen in Table 4. The exact description of the properties will be shown later in this chapter. Each sample was assigned a colour, under which is shown in graphs and XRD spectra.

Table 4: *Short characteristic of prepared samples.*

Freeze-casting	**Starting form**	**Freezing front velocity [µm/s]**	**Drying**	**Final form**
I-T 50_LYO	Ceramic suspension ICE-15 % HAP+S	3.4 ±0.3	Lyophilized (Freeze-dryer)	Porous scaffold
I-T 20_LYO		5.5 ±0.2		
V1_LYO		12.7 ±0.5		
V2_LYO		25.8 ±1.2		
V3_LYO		~ 1000		
I-T 50_AIR		3.4 ±0.3	Air-dried	Dense cast
I-T 20_AIR		5.5 ±0.2		
V1_AIR		12.7 ±0.5		
V2_AIR		25.8 ±1.2		
V3_AIR		~ 1000		
Classic shaping	**Starting form**	**Used pressure [MPa]**	**Processing**	**Final form**
SC	Ceramic suspension ICE-15% HAP+ S	-	Slip casting	Dense cast
UP 10 MPa	Calcined powder	10	Uniaxial pressing	Dense pellets
CIP 250 MPa		250	Cold isostatic pressing	
CIP 700 MPa		700		

5.1 Starting powders

Characterization of both, starting and the calcined powder was done, to observe the impact of calcination on phase composition and particle's size.

5.1.1 X-ray diffraction

The impact of calcination on phase composition can be seen in Figure 15. The XRD spectrum of commercial hydroxyapatite powder (HAP), contains one major phase which corresponds with the standard hydroxyapatite spectrum. Minor phase was identified as monetite ($CaHPO_4$). Two phases can be identified in the spectrum powder calcined at 800 °C for 1 hour (HAP C) – hydroxyapatite and β-TCP. The volume content of hydroxyapatite is significantly lower, compared to the starting powder, according to the Equation 3, is 30.9 vol.%.

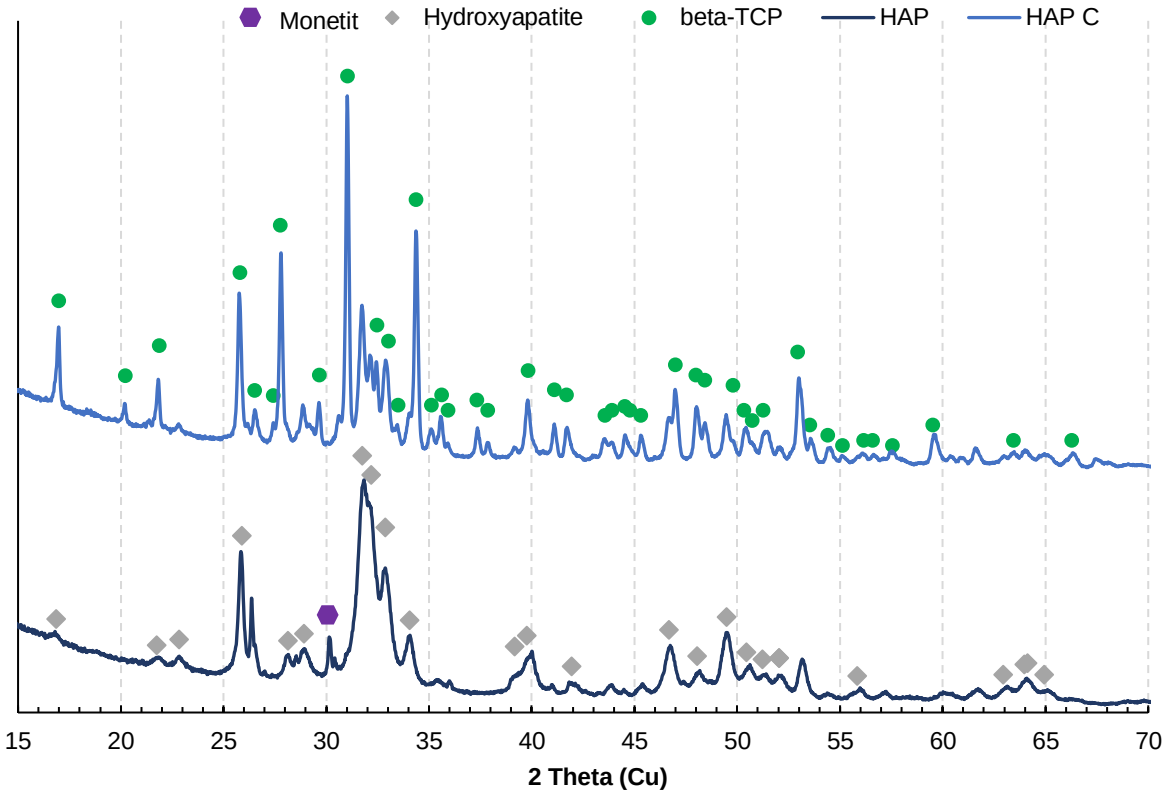

Figure 15: *XRD spectra of as received and calcined powder.*

5.1.2 Microstructure

Changes in microstructure can be seen in Figure 16. Calcination (800 °C/1 h) had a slight effect on the coarsening of ceramic particles. Starting powder (Figure 16a) contains a lower amount of agglomerates and higher amount of finer ceramic particles, compared to calcined powder (Figure 16b).

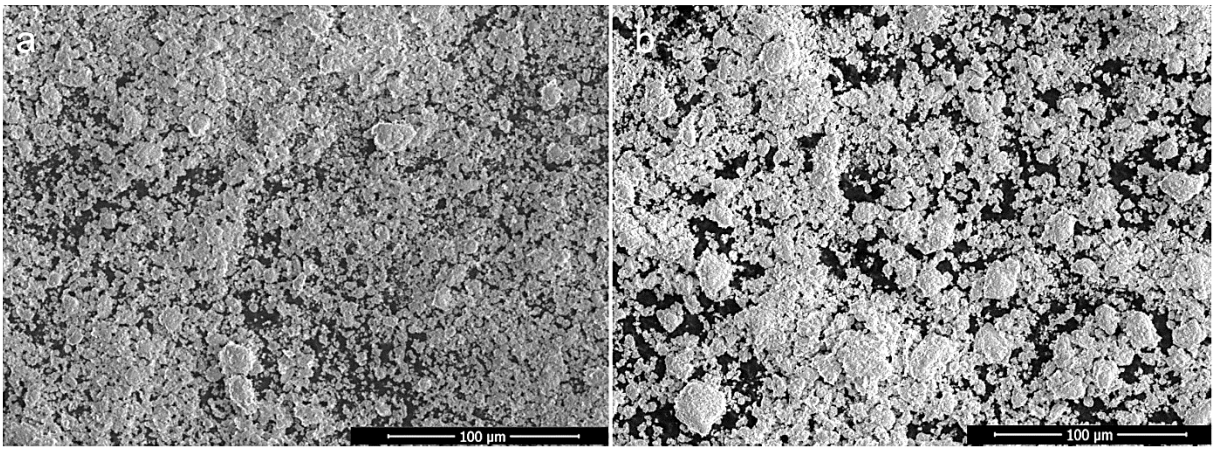

Figure 16: *Particles of used powders; a – starting hydroxyapatite powder; b – calcined powder.*

5.2 Samples prepared by freeze-casting

Porous and dense green bodies, as well as sintered samples prepared by freeze-casting, were characterized to obtain phase composition, microstructure, density and porosity.

5.2.1 X-ray diffraction

Effect of various freezing front velocities and types of drying on the phase composition of sintered samples was investigated.

Samples prepared by using the cooling plate

The XRD spectra (Figure 17) show that both air-dried and lyophilised samples, contain HA and β-TCP phases, whereas β-TCP is a major phase. However, the contents of individual phases are different. The content of HA in both air-dried samples (I-T 20_AIR and I-T 50_AIR) is higher (~ 24 vol.%) compared to HA abundance in lyophilised ones (~ 15 vol%). This fact is evident from the individual spectra – the intensity of HA peak (I_{100} (HA)) is higher in air-dried samples, and the intensity of HA peak is lower in lyophilised samples (I-T 20_LYO and I- T 50_LYO).

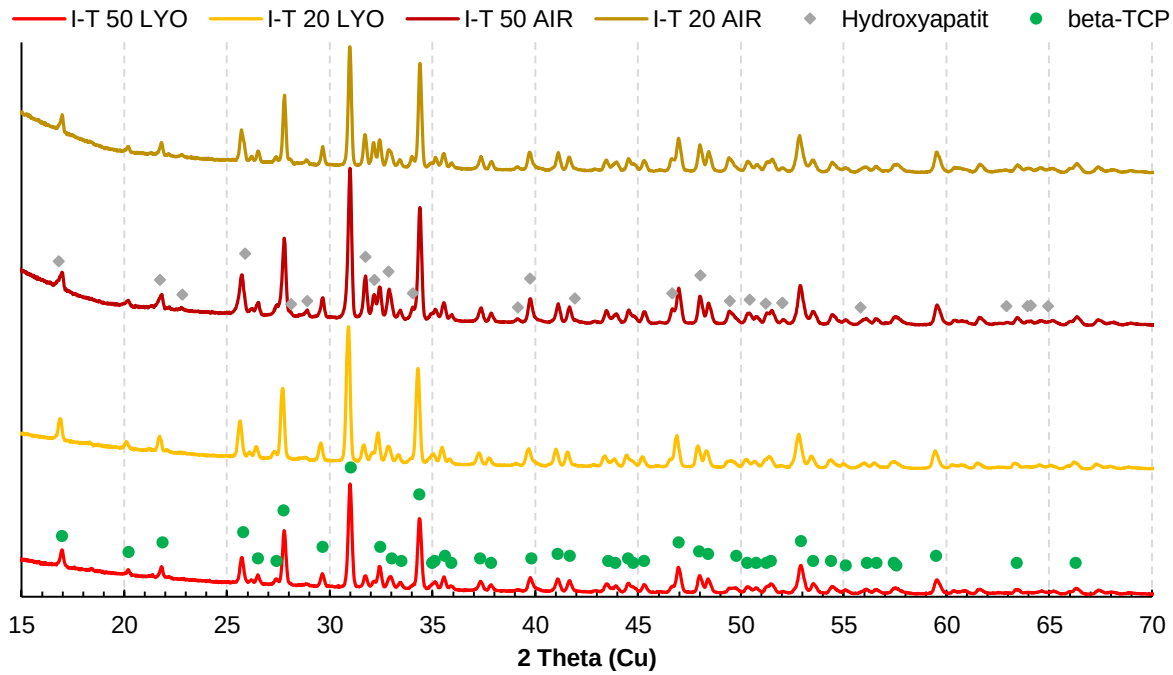

Figure 17: *XRD spectra of samples prepared by using the cooling plate.*

Samples prepared by using liquid nitrogen

The XRD spectra of lyophilised samples are presented in Figure 18. All samples contain both phases, hydroxyapatite and β-TCP. The β-TCP is also the major component, in this case. Content of HA phase decreases, as the freezing front velocity increases, see Table 5, so the highest content of HA is observed in the sample V1_LYO (~ 13 vol.%).

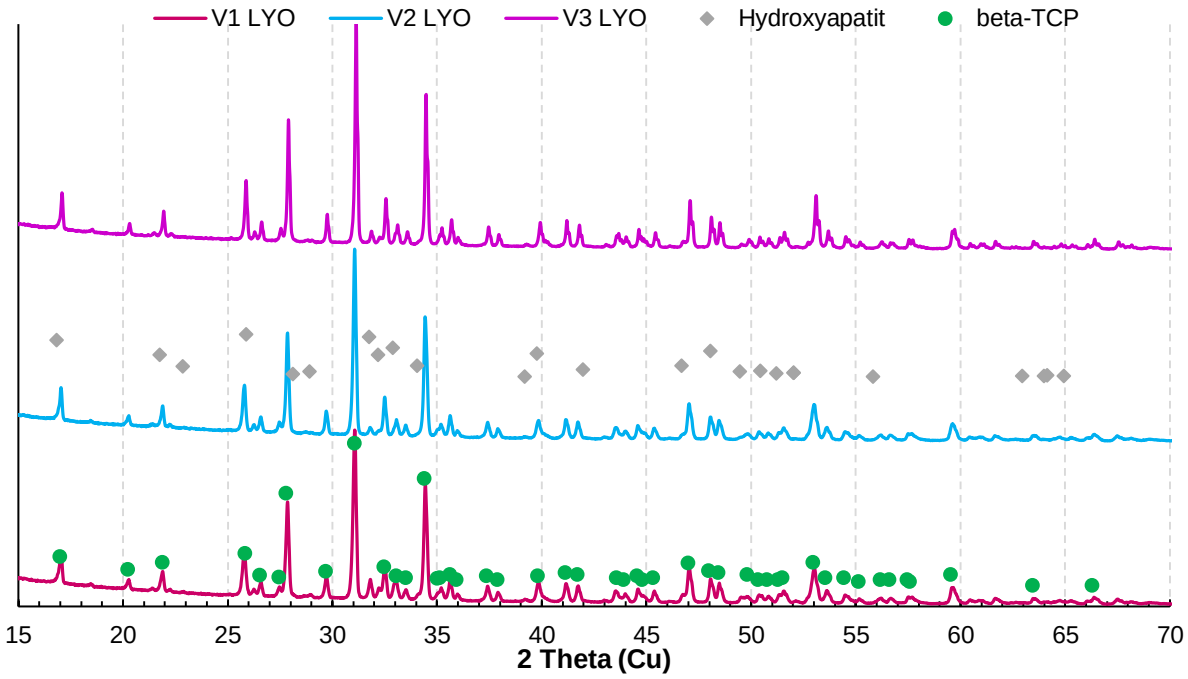

Figure 18: *XRD spectra of lyophilised samples prepared by using liquid nitrogen.*

Air-dried samples also consist of HA phase and β-TCP phase, with β-TCP being the major one, as in the case of lyophilised samples. However, the ratio of phases differs – the abundance of HA phase is higher, compared to lyophilised samples.

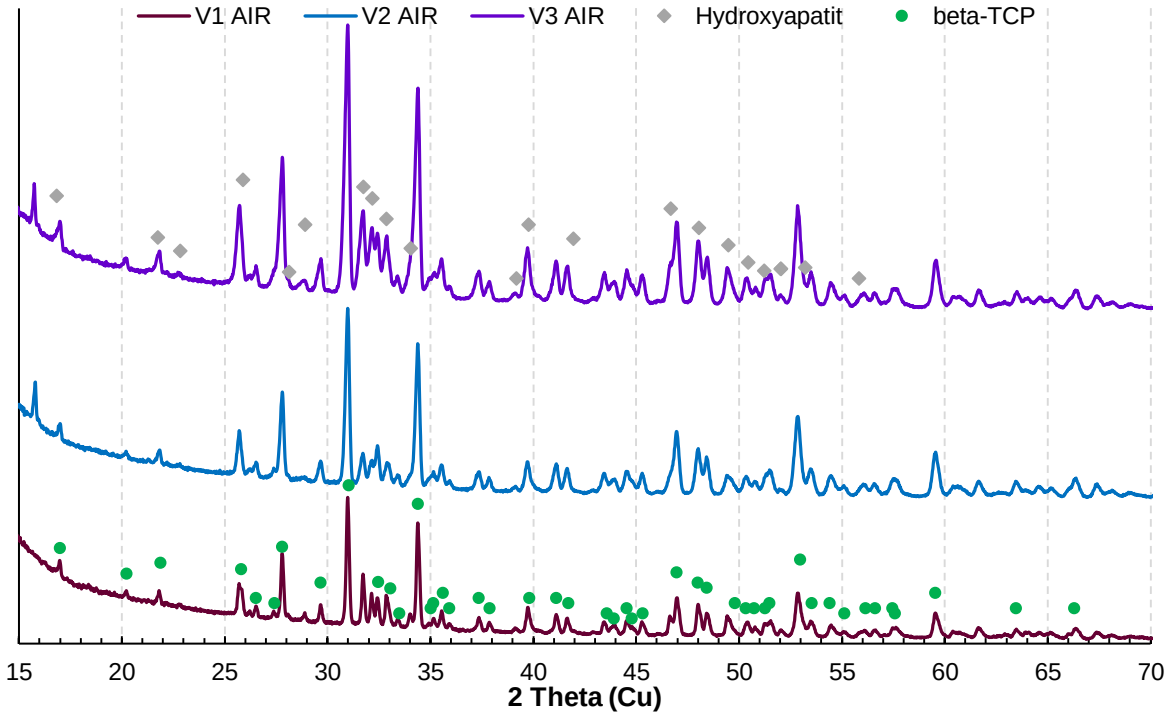

Figure 19: *XRD analysis of air-dried samples prepared by using liquid nitrogen.*

5.2.2 Microstructure

Porous samples

Interlamellar spaces and porosity were determined, as well as the content of HA in individual sintered samples (Table 5). It can be seen that size of interlamellar spaces decreases, as the freezing front velocity increases (Table 4). Content of HA decreases as the freezing front velocity increases, nevertheless the content of HA in samples frozen at the cooling plate is quite similar (~ 15.5 vol.%). Content of HA is similar also in the samples V2 and V3 (~ 7,4 vol.%).

Table 5: *Average values of interlamellar spaces, porosities and hydroxyapatite content of lyophilised freeze-cast samples.*

Sample – LYO	Interlamellar spaces [µm]	Porosity [%]	Content of HA [vol.%]
I-T 50	108.2 ±18.7	66.7 ±0.6	15.7
I-T 20	64.1 ±10.7	70.7 ±0.1	15.6
V1	45.0 ±7.6	72.3 ±0.0	13.3
V2	19.9 ±3.6	72.6 ±0.4	7.5
V3	-	66.9 ±0.3	7.4

Comparison of total porosities and the corresponding content of HA is shown in Figure 20. It can be observed that the content of HA decreases as the relative density decreases. The values of relative densities were derived from porosity (Table 5). However, this dependence applies to samples prepared by directional freezing, only therefore the sample V3 is an exception.

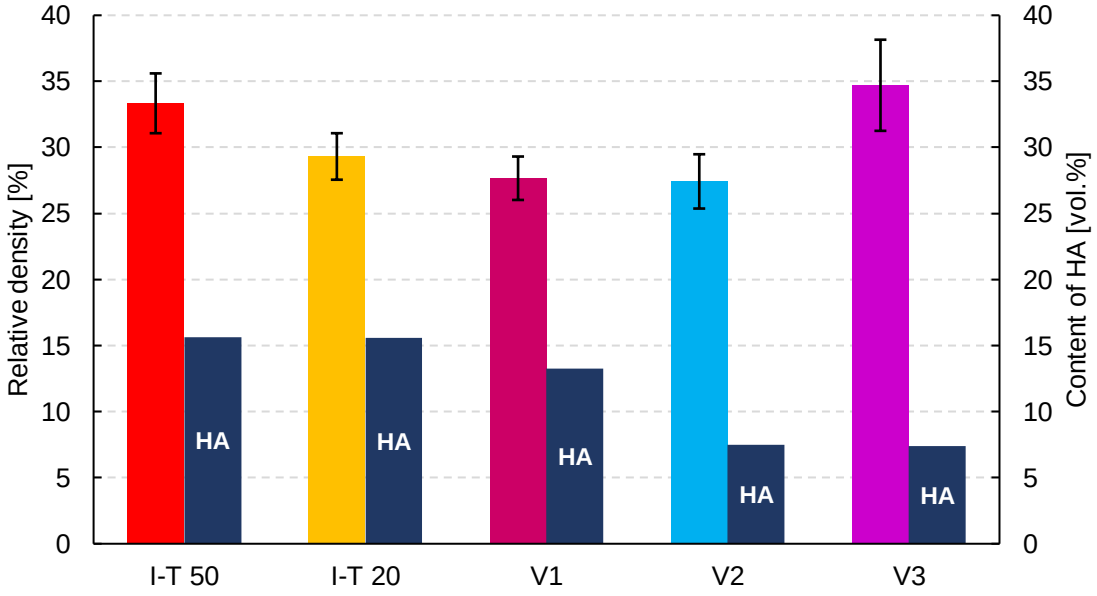

Figure 20: *Freeze-cast and lyophilized samples and comparison of their relative densities and hydroxyapatite contents after sintering.*

The microstructure of green bodies can be seen in Figure 21. The SEM micrographs were taken from the lamellae (I-T 20_LYO and V3), and it can be observed that there is slight difference in porosity between ceramic particles. Sample I-T 20_LYO is less compacted, compared to the sample V3_LYO, which is related to the values of porosity after sintering (Table 5). Ceramic particles of both samples seem to be homogenous in size, and no agglomerates can be observed.

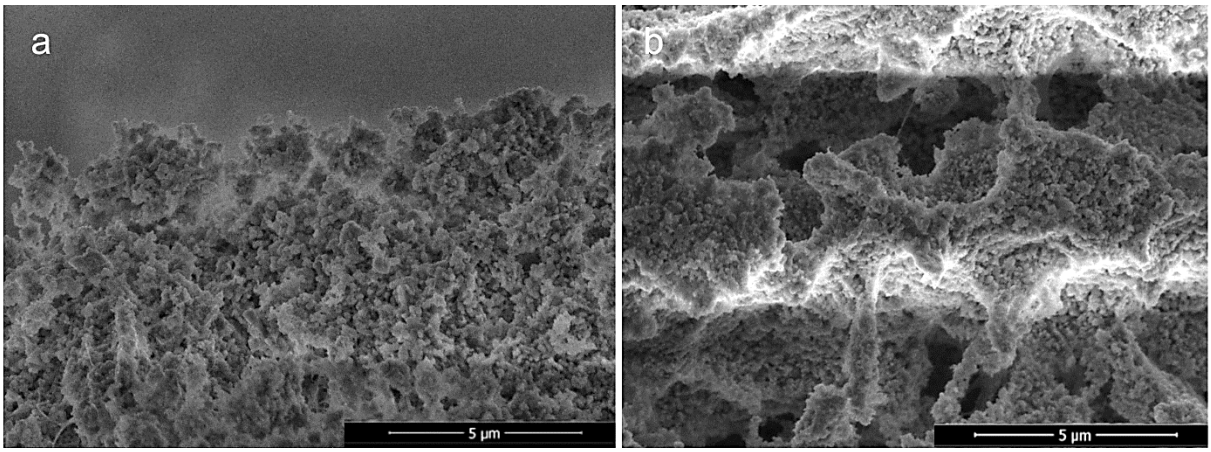

Figure 21: *Microstructure of green bodies lamellae; a – I-T 20_LYO; b –V3_LYO.*

The SEM micrographs of sintered samples were also taken (see Figure 22). It can be observed that sample I-T 50_LYO (Figure 22a) contains small pores between sintered ceramic particles, and these pores do not occur in other samples. A detail of the interlamellar bridge and its microstructure can be seen in Figure 22c, where two types of ceramic particles occur – bigger ones surrounded by a few number of smaller ones.

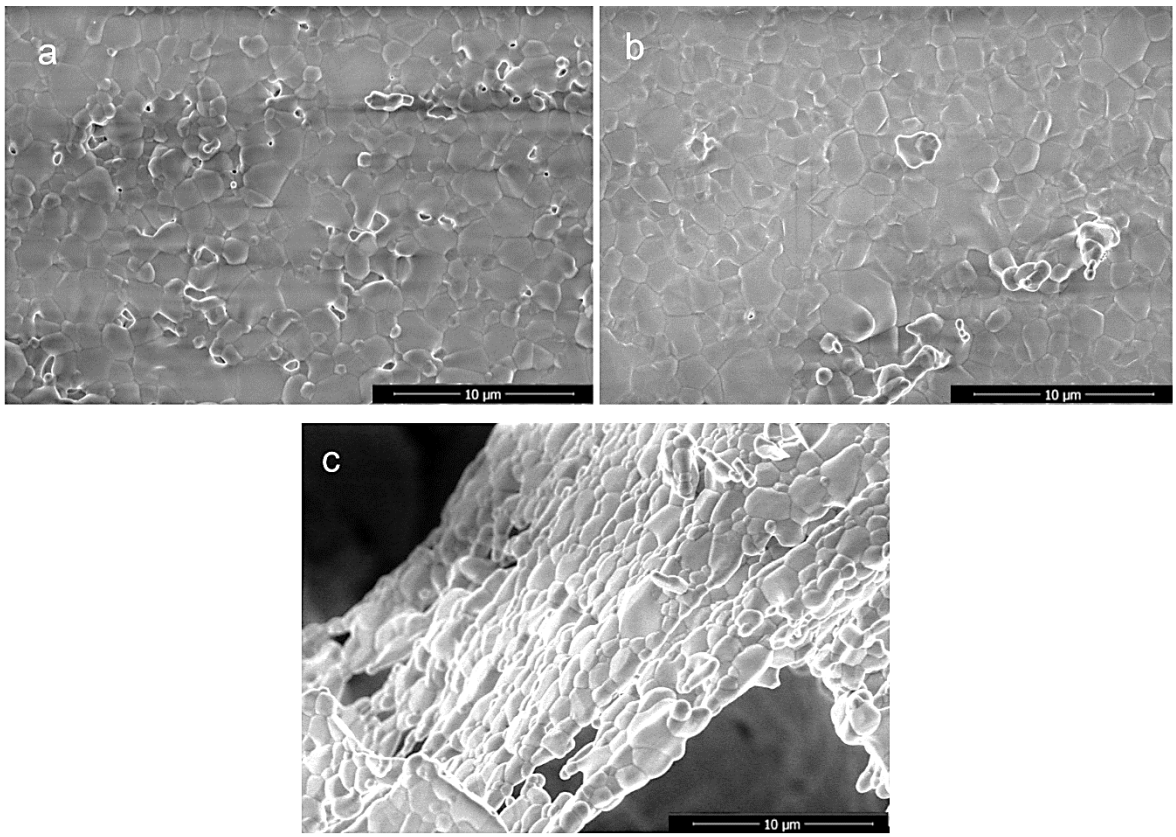

Figure 22: *Microstructure of sintered lamellae; a – I-T 50_LYO; b – I-T 20_LYO; c –V1_LYO (interlamellar bridge).*

Dense samples

Densities of green bodies, sintered samples and HA contents are shown in Table 6. Green body densities increase as the freezing rate increases. Final densities do not show such an exact trend, however, the most porous sample (I-T 50_AIR) was frozen with the slowest freezing rate. On the other hand, the highest green density can be observed in the sample, prepared by using liquid nitrogen.

Table 6: *Average values of green body densities, final densities and hydroxyapatite content of air-dried freeze-cast samples.*

Sample – AIR	Green body density [%]	Relative density [%]	Content of HA [vol.%]
I-T 50	38.9 ±0.3	89.1 ±0.6	24.7
I-T 20	44.3 ±0.4	97.2 ±0.4	24.4
V1	49.5 ±0.3	95.2 ±0.2	32.2
V2	52.8 ±0.5	98.2 ±0.8	20.7
V3	55.4 ±0.7	95.3 ±4.3	26.5

Comparison of relative densities and HA content can be seen in Figure 23. It can be observed that the content of HA in samples prepared by using the cooling plate (I-T 50_AIR and I-T 20_AIR) is almost the same. However, no significant trend can be observed in this case. Dependence of HA content on the final density of air-dried samples has not been proven in this case.

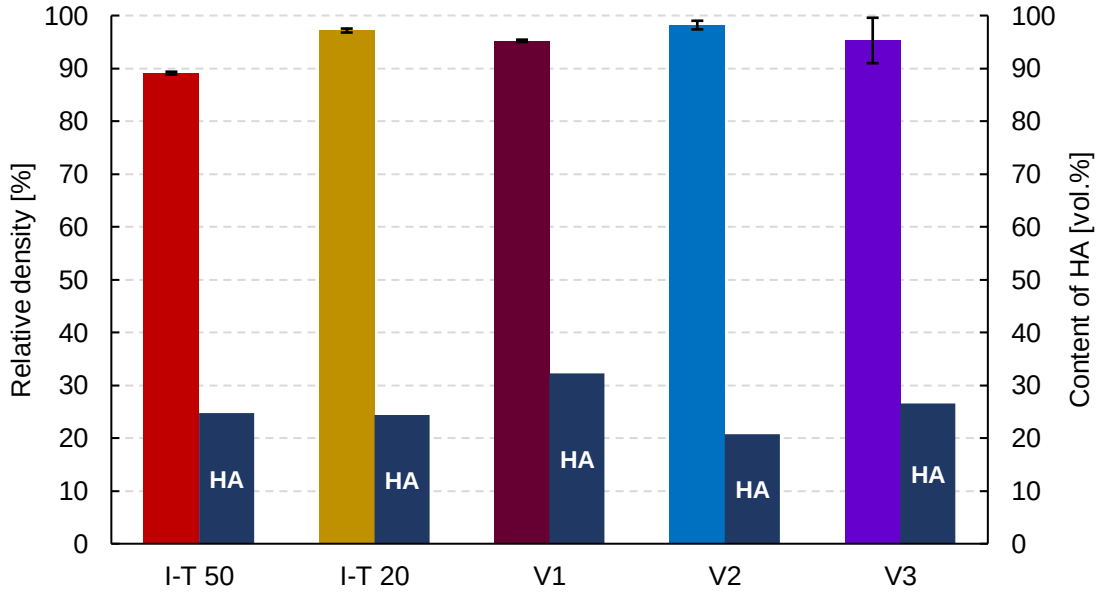

Figure 23: *Air-dried freeze-cast samples and comparison of their relative densities and hydroxyapatite contents after sintering.*

The SEM micrographs of green bodies with high green density can be seen in Figure 24. It can be observed that sample V1_AIR contains several agglomerates (Figure 24b). These agglomerates consist of small particles, which were not observed elsewhere in the sample. The surface of the sample I-T 50_AIR has slightly different microstructure. No agglomerates were observed, and the particles are more homogenous in size, see Figure 24a.

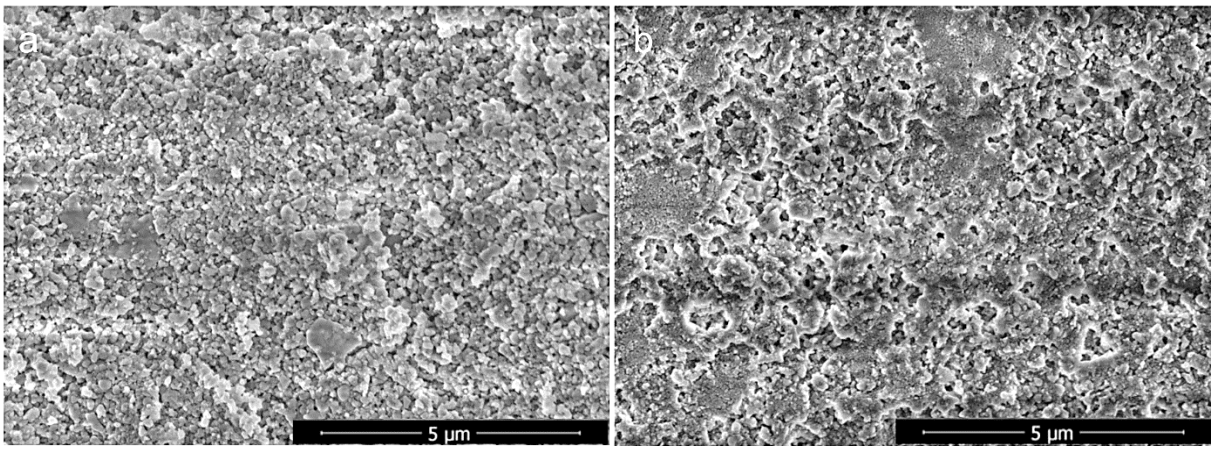

Figure 24: *Microstructure of dense green bodies; a – I-T 50_ AIR; b – V1_AIR.*

5.2.3 Mercury porosimetry

Porosimetry of freeze-cast samples, both air-dried and lyophilised was done. The dependence of pore volume on the pore radius can be seen in Figure 25. It can be seen that the air-dried sample (V3_AIR) contains only pores with size ranging between 10 and 100 nm. Sample V3_LYO contains two types of pores – smaller ones, with the size around 60 nm, and bigger ones, with the size around 1 µm. Those micron pores are the most represented, in the sample. It can be seen, that the measurement of sample V3_LYO was not completed, due to an incorrectly selected sample size. It can be observed that sample I-T 20_LYO contains pores with size primarily around 70 nm. However, interlamellar spaces measurements (Table 5) show that this sample contains also pores with the size around 65 µm, and these pores are out of the measurement range of porosimeter.

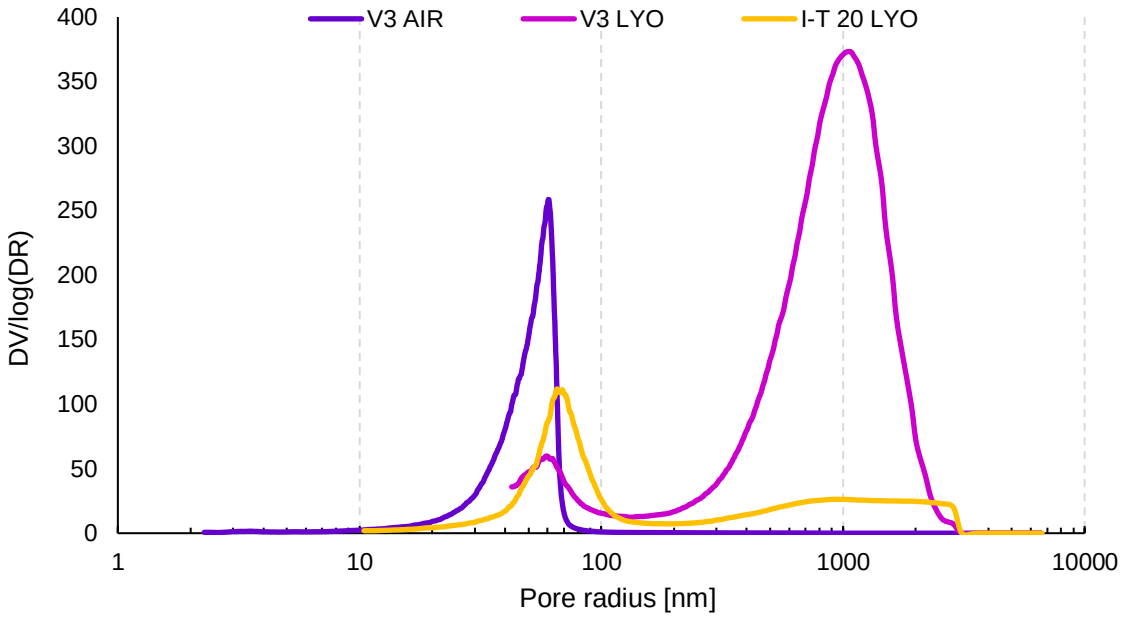

Figure 25: *Mercury porosimetry measurements of freeze-cast samples.*

5.3 Samples prepared by classic shaping methods

Green bodies and sintered samples prepared by slip-casting, uniaxial pressing and cold isostatic pressing were characterized from several aspects – phase composition, microstructure, density, etc.

5.3.1 X-ray diffraction

The impact of different processing on the phase composition of sintered samples can be seen in Figure 26. Presented XRD spectra differ in the content of HA and β-TCP phases. Isostatically pressed samples (CIP 700 MPa) contain the smallest amount of hydroxyapatite (~ 3.9 vol.%) and β-TCP is a major phase, which corresponds to the standard β-TCP spectrum. Other samples contain a higher amount of HA phase, and the amount increases as the pressure applied during processing decreases. The highest amount, approximately 20 vol.%, of hydroxyapatite, is present in slip-cast samples (SC).

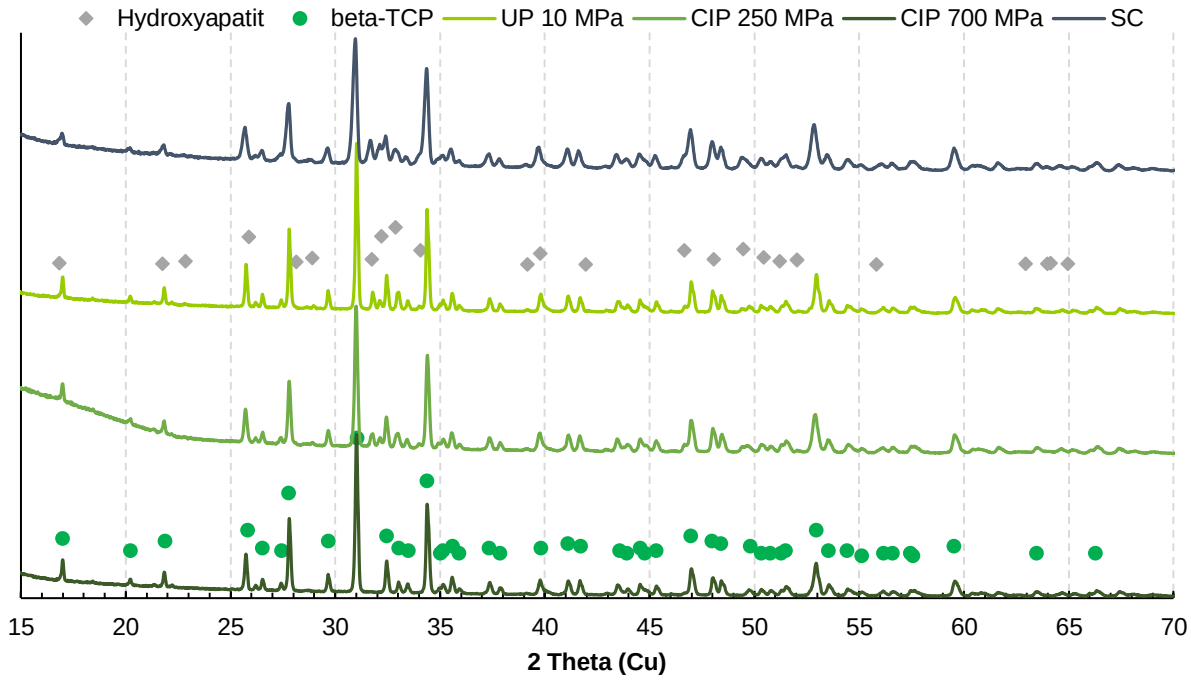

Figure 26: *XRD spectra of samples prepared by classic shaping methods.*

5.3.2 Microstructure and other characteristics

Densities of green bodies and sintered samples can be seen in Table 7, as well as a summary of HA content in sintered samples. As mentioned above, the content of HA phase in each sample differs due to the difference in applied pressures during preparation.

Table 7: *Average values of densities and corresponding hydroxyapatite content of samples prepared by classic shaping methods.*

Sample	Green body density [%]	Relative density [%]	Content of HA [%]
SC	46.6 ±0.6	98.9 ±0.6	19.9
UP 10 MPa	33.8 ±0.6	87.4 ±1.4	11.9
CIP 250 MPa	57.1 ±0.4	98.5 ±0.5	7.2
CIP 700 MPa	63.9 ±0.9	99.3 ±0.4	3.9

Comparison of relative density and HA content is shown in Figure 27. It can be observed that the content of HA is decreasing with the increase of the relative density of pressed samples. The sample prepared by slip-casting (SC) contains the highest amount of HA, despite a comparable value of relative density, compared to the isostatically pressed (CIP 700 MPa) ones.

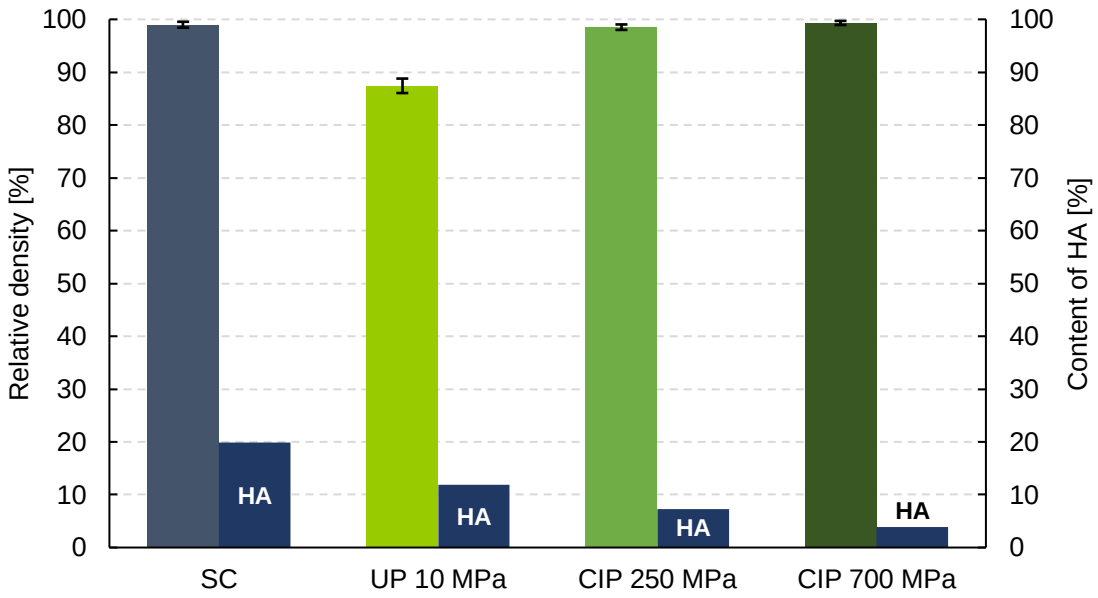

Figure 27: *Comparison of relative densities and related hydroxyapatite contents of samples prepared by classic shaping methods.*

There are no significant differences in microstructure of slip-cast green bodies and isostatically pressed (at 700 MPa) green bodies. The microstructure of both samples can be seen in Figure 28. The SEM micrographs were taken from the surface of green bodies, and several agglomerates can be observed in Figure 28b. The different distribution of pores and their size is not so obvious. This result is corresponding with values of relative densities after sintering. Values of relative densities (Table 7) are very similar – 98.9 vol.% for slip-cast sample, and 99.3 vol.% for the isostatically pressed sample at (700 MPa).

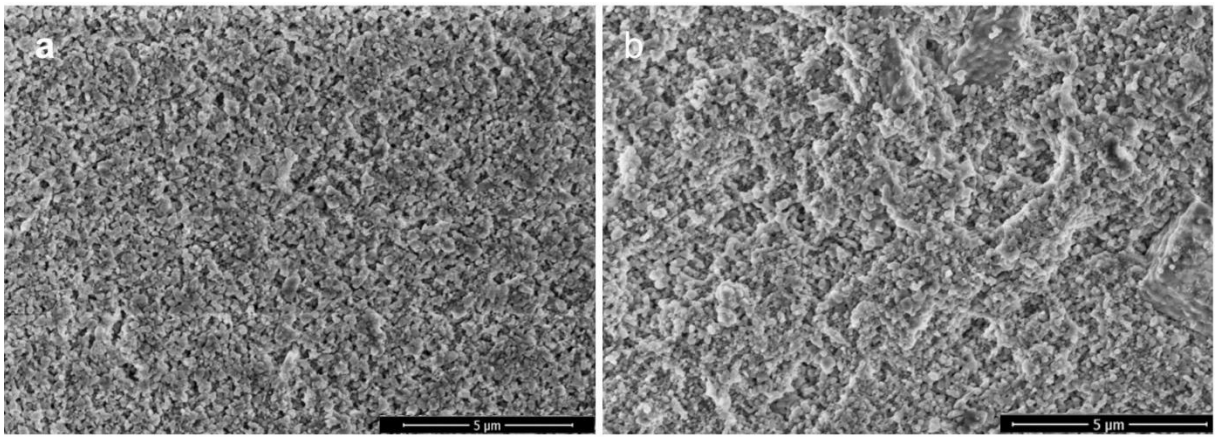

Figure 28: *Microstructure of green bodies; a – slip-cast sample; b – isostatically pressed samples at 700 MPa.*

5.3.3 Mercury porosimetry

Mercury porosimetry of green bodies (slip-cast and isostatically pressed samples) was performed to obtain the pore size and its volume representation. The pore distribution can be seen in Figure 29. It can be observed that all measured samples primarily contain pores with size ranging between 10 nm and 100 nm. The pore size decreases, with increasing applied pressure. The highest volume representation of pores in the isostatically pressed sample (CIP 250 MPa), can be also observed.

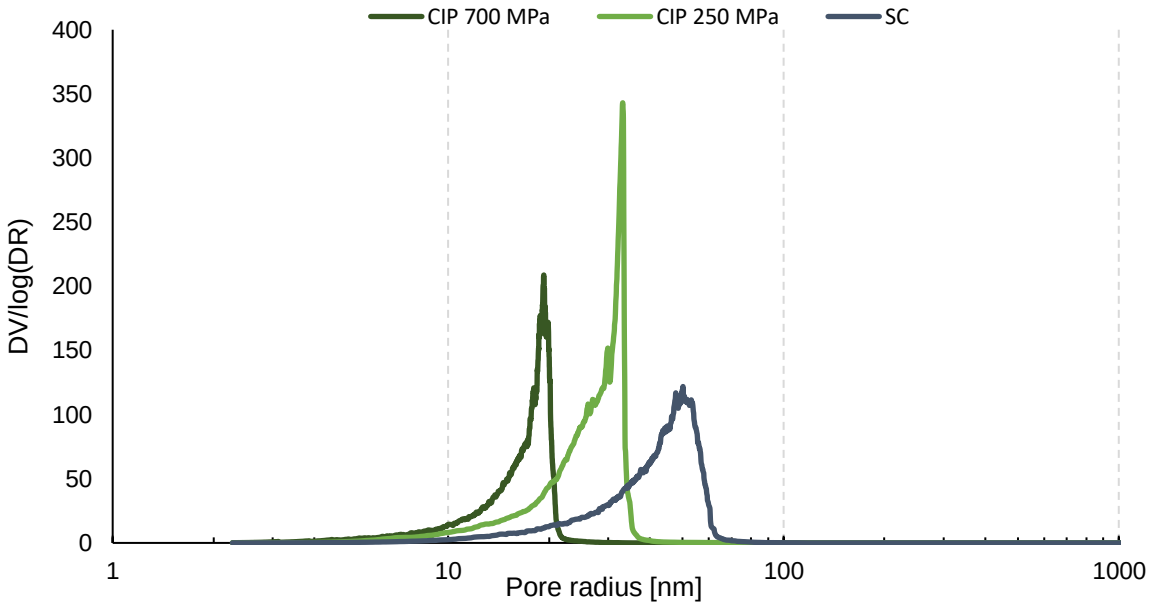

Figure 29: *Mercury porosimetry measurement of samples prepared by classic shaping methods.*

6 DISCUSSION

This part of the thesis is dedicated to the discussion of the obtained results. Especially, the effect of used shaping methods on microstructure and phase composition will be discussed.

6.1 Effect of used shaping method on resulting microstructure

Differences in microstructure, porosity and pore size, relative density, etc. were observed in samples prepared by several shaping methods.

Freeze-casting

Firstly, an influence of various freezing rates on porosity and size of interlamellar spaces was investigated. The results, shown in Table 5, revealed that the difference in the size of interlamellar spaces is caused by different velocities of freezing front, which corresponds with the literature [44, 51, 54]. It can be observed that total porosity (of sintered samples) increases with increasing freezing front velocity. This is caused by different size of intrelamellar spaces and pore distribution of green bodies, which is formed during freezing, the effect of various freezing velocities on pore distribution has already been described by Zheng et al [50]. These differences in porosity at the submicron level are affecting the kinetic of sintering process. The initial sintering temperature can be shifted, shrinkage kinetics changed, and sintered samples differ in total porosity. Different pore distribution in samples can also be observed in mercury porosimetry measurements (Figure 25).

The exception is the sample prepared by uncontrolled freezing (V3_ LYO). The structure of the sample is highly anisotropic. The characteristic lamellar structure could not be observed easily. The anisotropic structure of the sample V3_LYO is caused by the rapid freezing of ceramic suspension, however, it was observed that the sample contains certain parts with lamellar structure (Figure 30). Observed lamellae are very thin (approx. 5 μm in the green body), however lamellar structure is not consistently distributed throughout the whole sample and represents a minor fraction of total porosity.

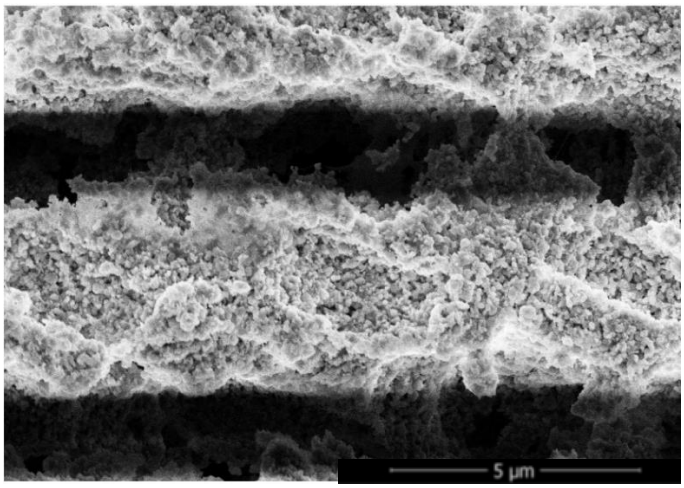

Figure 30: *Detail of lamellar structure in green body V3_LYO.*

Furthermore, an influence of the used type of drying on the resulting microstructure was investigated. Lyophilised samples (after sintering) are highly porous (~ 70 %), with characteristic lamellar structure, which is preserved during the lyophilisation. Ice sublimation in vacuum ensures that the sample's structure remains stable. On the other hand, the air-dried samples are dense, after sintering. Ice crystals formed during freezing melt, the whole structure is thawed and collapses. The remaining water then evaporates spontaneously during drying. Relative densities of the green bodies range between 40 % and 55 %. These values are relatively high, and it can be assumed that high pressure on ceramic particles was induced during freezing [50]. Relative densities, approximately at 90 %, after sintering (Table 6), are almost comparable with relative densities of samples prepared by classic shaping methods (Table 7).

Porosimetry

Mercury porosimetry measurements of green bodies revealed that all freeze-cast and air-dried samples and samples prepared by classic shaping methods have a unimodal pore size distribution, with pore radius ranging between 10 and 100 nm, see Figure 31 (samples SC and V3_AIR).

Lyophilized samples show bimodal pore size distribution, with two different pore sizes. Smaller type of pore radius ranges between 10 and 100 nm. Size of bigger pores is influenced by freezing front velocity. Decreasing of freezing front velocity increases the size of interlamellar spaces. In the case of V3_LYO sample, size of interlamellar spaces is mostly around 1 µm (Figure 31), this corresponds with observed lamellar porosity (Figure 30). Size of interlamellar spaces in sample I-T 20_LYO is much higher (~ 65 µm). Such big pores are out of the measuring range of the used porosimeter.

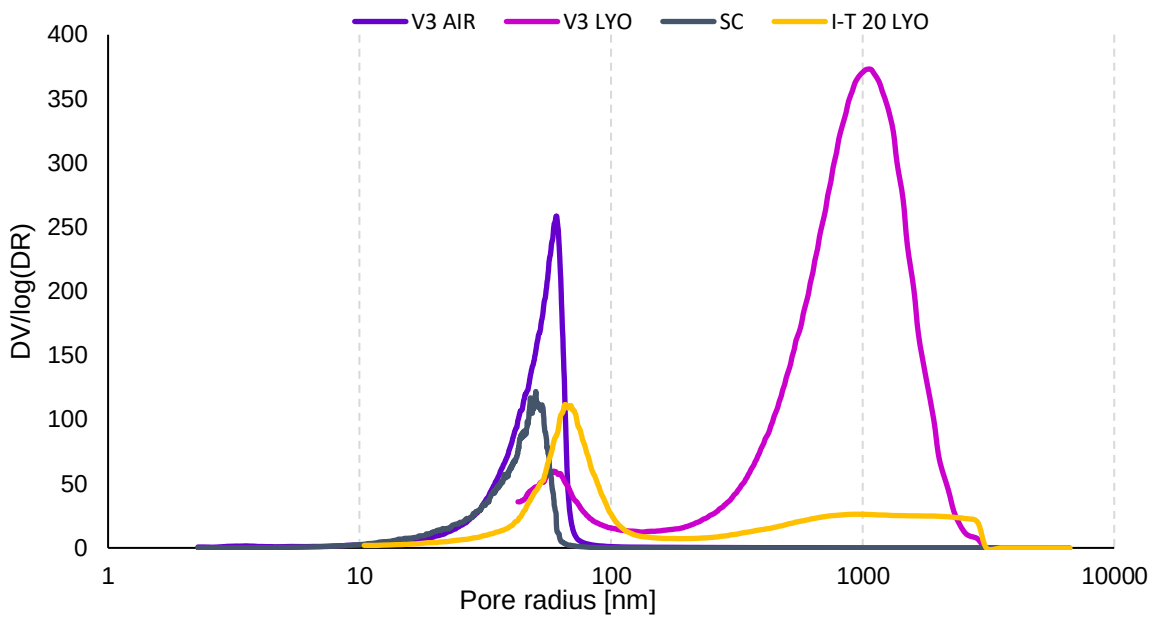

Figure 31: *Comparison of mercury porosity measurements.*

Classic shaping methods

Influence of applied external pressure on the resulting microstructure was also investigated. It is apparent that cold isostatic pressing provides samples with the highest values of green body densities, between 57 % (CIP 250 MPa) and 64 % (CIP 700 MPa). Such high values were achieved due to the high pressure, and thanks to good compressibility of HA powder. Sintered samples show also very high values of relative densities, which increase with increasing pressure. The exception is a slip-cast sample. Green body density of the slip-cast sample is considerably lower (46 %) compared to isostatically pressed samples. The relative density after sintering reaches more than 98 %, even if no pressure was applied during sample preparation. Such a high value was achieved by the high temperature of sintering (1200 °C) and long dwell time (120 min). It can be assumed that during a long dwell time at 1200 °C is grain growth sufficient to compensate the differences in green body densities. It is also necessary to consider the fact that the pressed samples were prepared from calcined powder, which was not further processed (milling). The slip-cast samples were prepared from a water-based suspension, which was milled for at least 24 hours. Therefore, the pore distribution is slightly different in the slip-cast samples, compared to isostatically pressed ones. This fact is apparent from mercury porosimetry measurement (Figure 29), which shows that slip-cast sample pore distribution is not so narrow as in the case of isostatically pressed samples.

Effect of milling

Influence of powder milling on the resulting microstructure was observed. The microstructure of the isostatically pressed sample (at 700 MPa) shown in Figure 28b revealed, that samples prepared without previous powder milling, contain prismatic agglomerates. These agglomerates were also observed in the used powder, as well as in samples prepared by uniaxial pressing at 10 MPa, and isostatic pressing at 250 MPa, see Figure 32.

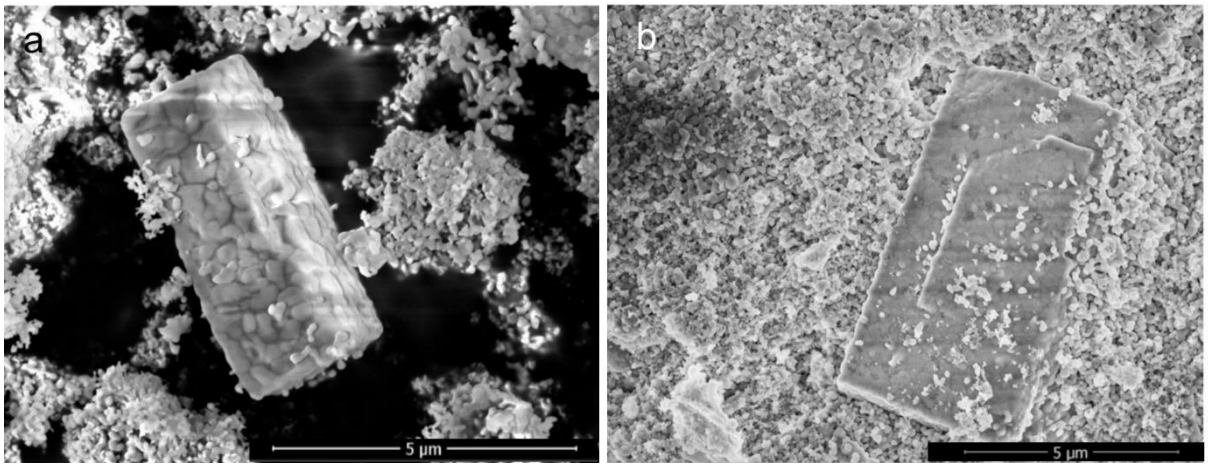

Figure 32: *Prismatic agglomerates; a – in calcined hydroxyapatite powder; b – isostatically pressed sample at 250 MPa.*

No similar agglomerates were observed in freeze-cast or slip cast samples. Therefore, it can be assumed that present agglomerates were milled down during suspension milling. It is apparent that the ball milling changes the calcined powder microstructure, which can further affect the sintering kinetics, and the final properties of sintered samples. However, in this research, no significant changes in investigated properties were observed.

6.2 Changes in phase composition

Influence of the used preparation method on the phase composition of sintered samples was investigated by X-ray diffractometry and Raman spectroscopy. Process of hydroxyapatite phase transformation is very complex, and it is difficult to determine the exact processing parameter, which leads to the obtained content of HA in samples. Influence of processing on final phase composition is shown in Figure 33, and it is apparent that used shaping method influences hydroxyapatite phase transition because individual samples differ in the intensity of HA peak (I_{100} (HA)).

To eliminate different temperature conditions for HA phase transformation, all samples were sintered at 1200 °C for 120 min. At this temperature, HA decomposes into β-TCP and other several CaP compounds (α-TCP, CaO, etc.), which are unstable at this temperature [65, 66]. Therefore, no other phases can be found in these samples, except HA and β-TCP.

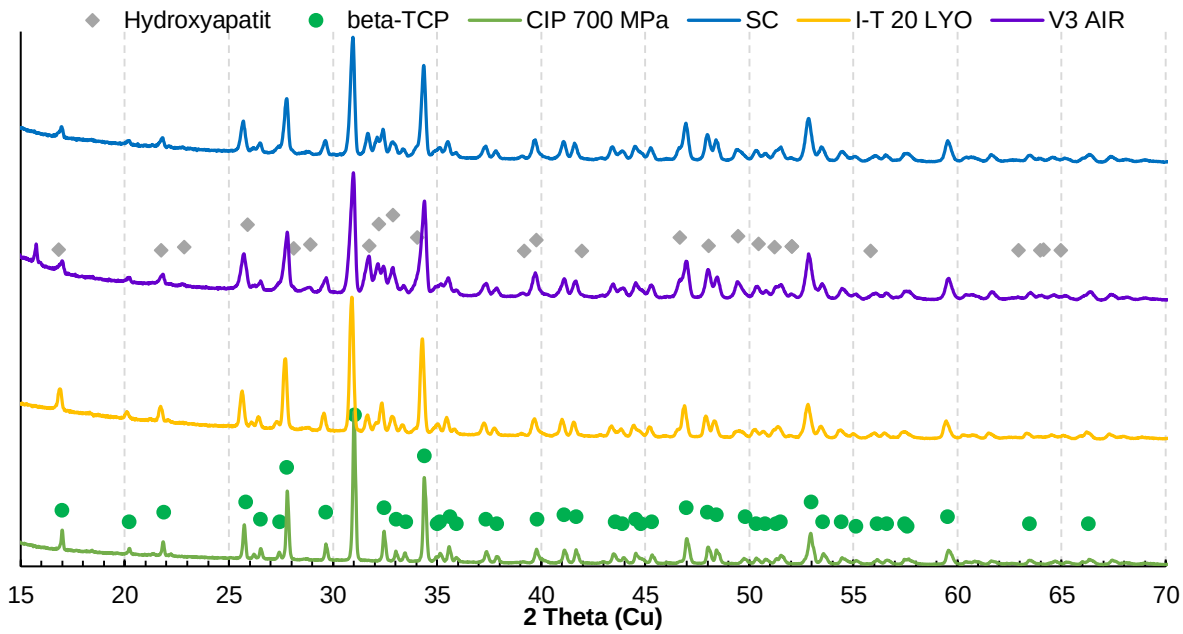

Figure 33: *Comparison of XRD analysis of sintered samples prepared by various methods.*

Effect of the calcination process

Firstly, an influence of powder calcination was investigated. The results shown in Figure 15 indicate that the powder calcination at 800 °C for 1 hour, induces the early phase transition of HA to β-TCP. HA is dehydroxylated during the calcination process. The dehydroxylation of HA begins at 630 °C and intensifies with increasing temperature, β-TCP is formed and becomes the major phase. Nevertheless, the dehydroxylation process can only take place up to the calcination temperature of 800 °C, and it is not possible to achieve the complete transformation of HA into β-TCP at this temperature. The effect of calcination on phase transition of HA has already been described in the literature [63, 64, 65] and partial transition of HA obtained in this research correspond with those results.

Influence of used freezing rate and drying

The influence of the freezing front velocity on HA content was investigated. The results shown in Figure 20 revealed that the content of HA decreases with increasing freezing front velocity and ranges between 7 vol.% (V2_LYO, V3_LYO) and 15 vol.% (I-T 50_LYO, I-T 20_LYO, V1_LYO). The air-dried samples show significantly higher content of HA. The results shown in Figure 23 revealed that the difference in HA content between lyophilized and air-dried samples is more than 10 vol.%. No significant trend related to the freezing front velocity can be observed here. The difference between lyophilized and air-dried samples can be seen in XRD spectra (Figure 34). It is also apparent that the intensity of HA peak (I_{100} (HA)) is higher in the air-dried samples, than in the lyophilised ones.

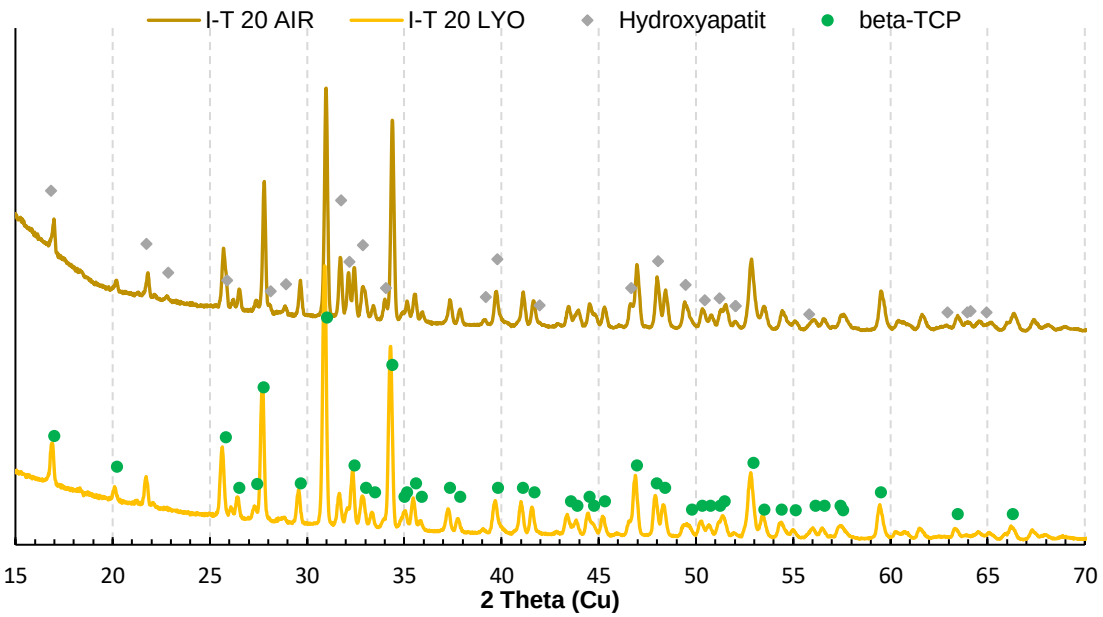

Figure 34: *Comparison of XRD spectra of lyophilized and air-dried samples.*

It can be concluded that the lyophilization process, used for porous scaffolds preparation, is significantly affecting the final phase composition of samples. Besides, the effect of used freezing rate is apparent only in lyophilized samples, containing the macropores.

Effect of milling and applied pressure

The slip-cast samples contain the highest amount of HA – approximately 20 vol.%, compared to other samples prepared by classic shaping methods. However, it is necessary to include the fact that the sample was prepared by casting the ceramic suspension, which was milled at least for 24 hours. Due to the different microstructure of ceramic powder, sintering kinetics can be changed. Therefore, the phase transition of HA cannot proceed in the same way as in the case of samples prepared by pressing methods. Slip-cast sample is comparable with freeze-cast and air-dried samples, due to the similarities in processing, resulting microstructure and content of HA.

Samples prepared by uniaxial pressing and isostatic pressing shown decreasing content of HA with increasing pressure. Isostatically pressed samples at 700 MPa (CIP 700 MPa) shown the lowest content of HA (~ 3 vol.%). Isostatic pressing at such high pressure affects the ceramic particle redistribution and the whole process is similar to the initial stage of sintering [9]. Thus, the applied pressure induced the phase transition of the remaining hydroxyapatite into β-TCP and obtained samples may contain such a low amount of HA. However, impact of applied pressure on HA content will be further investigated in isostatically pressed green bodies.

Raman spectroscopy

Additional analysis by Raman spectroscopy was performed, to confirm the presence of HA and β-TCP. The doublet peak with Raman shift between 900 and 1000 cm^{-1} can be seen in Figure 35. This doublet peak which can be observed in the Raman spectrum of β-TCP represents a PO_4^{3-} group and its specific bonding in the crystalline structure of β-TCP. Group of peaks with Raman shift around 600 cm^{-1} also belongs to PO_4^{3-} group (P–O bond). Peak with Raman shift around 400 cm^{-1} represents a bond between Ca^{2+} and PO_4^{3-}, which belongs to both HA and β-TCP [67, 68, 69]. No more characteristic Raman shifts of HA were observed in none of the measured samples, which could be caused by high intensity of doublet peak representing β-TCP. However, these measurements were only preliminary, and distribution of phases in presented biphasic system will be further investigated by Raman spectroscopy.

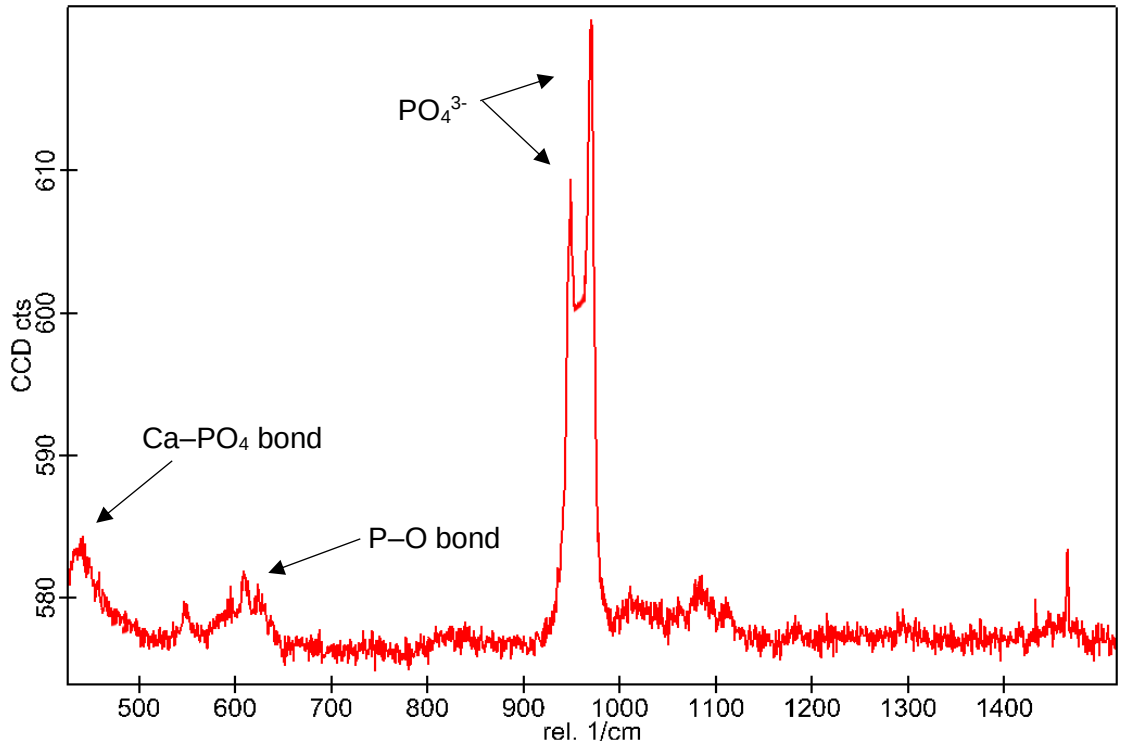

Figure 35: *Raman spectrum of sintered sample I-T 20_LYO.*

7 CONCLUSIONS

Porous and dense samples have been successfully prepared by several shaping methods. Impact of shaping method can be observed on green body density, relative density and porosity, as well as on the content of hydroxyapatite after sintering.

- Phase transition of hydroxyapatite into β-TCP was already observed during the calcination process at 800 °C for 1 hour. The ceramic powder used for samples preparation was a biphasic mixture, containing ~ 30 vol.% of hydroxyapatite.

- Raman spectroscopy was successfully used to identify β-TCP peaks and the method will be further used as a comparative method for the phase distribution investigation. The map of the sample's surface can be created and revealed to the distribution of individual phases.

- The mercury porosimetry results revealed differences in the microstructure, especially in samples with high green body density. Obtained results correlated with SEM analysis of green bodies. Bimodal pore size distribution was obtained in all lyophilized green bodies, including the samples without lamellae.

- Differences in the green density can be compensated during the sintering at 1200 °C for 120 min, so the values of relative densities after sintering are almost equal in dense samples, despite the initial differences.

- It was observed that the hydroxyapatite content is increasing with increasing porosity, as well as with the pore size. This trend was observed for samples with unimodal pore size distribution as well as for samples with bimodal pore size distribution. Content of HA varies from 3 vol.% to 30 vol.% for samples with unimodal pore size distribution, and from 7 vol.% to 15 vol.% for samples with bimodal por size distribution.

8 LIST OF REFERENCES

[1] Nagaich, Upendra. “Current trends in bone tissue regeneration.” *Journal of advanced pharmaceutical technology & research* vol. 8,2 (2017): 45. doi: 10.4103/japtr.JAPTR_10_17.

[2] WANG, Xiaojian, Shanqing XU, Shiwei ZHOU, et al. Topological design and additive manufacturing of porous metals for bone scaffolds and orthopaedic implants: A review. *Biomaterials*. 2016, 83, 127-141. DOI: 10.1016/j.biomaterials.2016.01.012. ISSN 01429612. Available at: https://linkinghub.elsevier.com/retrieve/pii/S0142961216000144.

[3] KROEZE, Robert, Marco HELDER, Leon GOVAERT and Theo SMIT. Biodegradable Polymers in Bone Tissue Engineering. *Materials*. 2009, **2**(3), 833-856. DOI: 10.3390/ma2030833. ISSN 1996-1944. Available at: http://www.mdpi.com/1996-1944/2/3/833

[4] MULCHANDANI, Neha, Arbind PRASAD and Vimal KATIYAR. Resorbable polymers in bone repair and regeneration. *Materials for Biomedical Engineering*. Elsevier, 2019, 2019, 87-125. DOI: 10.1016/B978-0-12-818415-8.00004-8. ISBN 9780128184158.
Available at: https://linkinghub.elsevier.com/retrieve/pii/B9780128184158000048

[5] LONG, Marc and H.J RACK. Titanium alloys in total joint replacement—a materials science perspective. *Biomaterials*. 1998, 19(18), 1621-1639. DOI: 10.1016/S0142-9612(97)00146-4. ISSN 01429612. Available at: https://linkinghub.elsevier.com/retrieve/pii/S0142961297001464

[6] PIELICHOWSKA, Kinga and Stanislaw BLAZEWICZ. Bioactive Polymer/Hydroxyapatite (Nano)composites for Bone Tissue Regeneration. *Biopolymers*. Berlin, Heidelberg: Springer Berlin Heidelberg, 2010, 2010-4-21, s. 97-207. Advances in Polymer Science.
DOI: 10.1007/12_2010_50. ISBN 978-3-642-13629-0.
Available at: http://link.springer.com/10.1007/12_2010_50

[7] NIXON, Alan J. Bone Grafts and Bone Substitutes. *Equine fracture repair*. 2nd edition. Hoboken, NJ: Wiley-Blackwell, 2020, 2019-10-28, s. 163-172. DOI: 10.1002/9781119108757. ISBN 9781119108757.

[8] VALLET-REGÍ, María and Antonio J. SALINAS. Ceramics as bone repair materials. Bone Repair Biomaterials. Elsevier, 2019, 2019, s. 141-178. DOI: 10.1016/B978-0-08-102451-5.00006-8. ISBN 9780081024515.
Available at: https://linkinghub.elsevier.com/retrieve/pii/B9780081024515000068

[9] CARTER, C. Barry and M. Grant NORTON. *Ceramic materials: science and engineering*. New York: Springer, 2007. ISBN 03-874-6270-8.

[10] KUCKO, Nathan W., Ralf-Peter HERBER, Sander C.G. LEEUWENBURGH and John A. JANSEN. Calcium Phosphate Bioceramics and Cements. *Principles of Regenerative Medicine*. Elsevier, 2019, 2019, 591-611. DOI: 10.1016/B978-0-12-809880-6.00034-5. ISBN 9780128098806.
Available at: https://linkinghub.elsevier.com/retrieve/pii/B9780128098806000345

[11] JEONG, Jiwoon, Jung Hun KIM, Jung Hee SHIM, Nathaniel S. HWANG and Chan Yeong HEO. Bioactive calcium phosphate materials and applications in bone regeneration. *Biomaterials Research*. 2019, **23**(1), 1-11. DOI: 10.1186/s40824-018-0149-3. ISSN 2055-7124.
Available at: https://biomaterialsres.biomedcentral.com/articles/10.1186/s40824-018-0149-3
[12] C. CHOW, Laurence. Next generation calcium phosphate-based biomaterials. *Dental Materials Journal*. 2009, **28**(1), 1-10. DOI: 10.4012/dmj.28.1. ISSN 1881-1361.
Available at: http://joi.jlc.jst.go.jp/JST.JSTAGE/dmj/28.1?from=CrossRef
[13] T., Albrektsson and Johansson C. Osteoinduction, osteoconduction and osseointegration. *European Spine Journal*. 2001, **10**, S96-S101. DOI: 10.1007/s005860100282. ISSN 0940-6719.
Available at: http://link.springer.com/10.1007/s005860100282
[14] ABIDI, Syed Sibte Asghar and Qasim MURTAZA. *Synthesis and Characterization of Nano-hydroxyapatite Powder Using Wet Chemical Precipitation Reaction*. 2014, **30**(4), 307-310. DOI: 10.1016/j.jmst.2013.10.011. ISSN 10050302.
Available at: https://linkinghub.elsevier.com/retrieve/pii/S1005030213002387
[15] HUANG, J., S. M. BEST, W. BONFIELD, R. A. BROOKS, N. RUSHTON, S. N. JAYASINGHE and M. J. EDIRISINGHE. In vitro assessment of the biological response to nano-sized hydroxyapatite. *Journal of Materials Science: Materials in Medicine*. 2004, **15**(4), 441-445. DOI: 10.1023/B:JMSM.0000021117.67205.cf. ISSN 0957-4530.
Available at: http://link.springer.com/10.1023/B:JMSM.0000021117.67205.cf
[16] ŠUPOVÁ, Monika. Isolation and Preparation of Nanoscale Bioapatites from Natural Sources: A Review. *Journal of Nanoscience and Nanotechnology*. 2014, **14**(1), 546-563.
DOI: 10.1166/jnn.2014.8895. ISSN 15334880.
[17] SZCZEŚ, Aleksandra, Lucyna HOŁYSZ and Emil CHIBOWSKI. Synthesis of hydroxyapatite for biomedical applications. *Advances in Colloid and Interface Science*. 2017, **249**, 321-330. DOI: 10.1016/j.cis.2017.04.007. ISSN 00018686.
Available at: https://linkinghub.elsevier.com/retrieve/pii/S0001868617300957
[18] OKADA, Masahiro and Takuya MATSUMOTO. Synthesis and modification of apatite nanoparticles for use in dental and medical applications. *Japanese Dental Science Review*. 2015, **51**(4), 85-95. DOI: 10.1016/j.jdsr.2015.03.004. ISSN 18827616.
Available at: https://linkinghub.elsevier.com/retrieve/pii/S1882761615000186
[19] CARRODEGUAS, R.G. and S. DE AZA. A-Tricalcium phosphate: Synthesis, properties and biomedical applications. Acta Biomaterialia. 2011, 7(10), 3536-3546. DOI: 10.1016/j.actbio.2011.06.019. ISSN 17427061.
Available at: https://linkinghub.elsevier.com/retrieve/pii/S174270611100256X

[20] SAKAI, Kana, Yoshiya HASHIMOTO, Shunsuke BABA, Aki NISHIURA and Naoyuki MATSUMOTO. Effects on bone regeneration when collagen model polypeptides are combined with various sizes of alpha-tricalcium phosphate particles. *Dental Materials Journal*. 2011, **30**(6), 913-922. DOI: 10.4012/dmj.2011-126. ISSN 0287-4547.
Available at: https://www.jstage.jst.go.jp/article/dmj/30/6/30_2011-126/_article
[21] KOBAYASHI, Nobuhiro, Yoshiya HASHIMOTO, Akihisa OTAKA, Tetsuji YAMAOKA and Shosuke MORITA. Porous Alpha-Tricalcium Phosphate with Immobilized Basic Fibroblast Growth Factor Enhances Bone Regeneration in a Canine Mandibular Bone Defect Model. *Materials*. 2016, **9**(10), 1-11. DOI: 10.3390/ma9100853. ISSN 1996-1944.
Available at: http://www.mdpi.com/1996-1944/9/10/853
[22] MATSUNAGA, Katsuyuki, Tomonori KUBOTA, Kazuaki TOYOURA and Atsutomo NAKAMURA. First-principles calculations of divalent substitution of Ca^{2+} in tricalcium phosphates. *Acta Biomaterialia*. 2015, **23**, 329-337. DOI: 10.1016/j.actbio.2015.05.014. ISSN 17427061. Available at: https://linkinghub.elsevier.com/retrieve/pii/S174270611500238X
[23] L., Galois, Mainard D. and Delagoutte J. Beta-tricalcium phosphate ceramic as a bone substitute in orthopaedic surgery. International Orthopaedics. 2002, 26(2), 109-115. DOI: 10.1007/s00264-001-0329-x. ISSN 0341-2695.
Available at: http://link.springer.com/10.1007/s00264-001-0329-x
[24] PETERS, F. and D. REIF. Functional Materials for Bone Regeneration from Beta-Tricalcium Phosphate. *Materialwissenschaft und Werkstofftechnik*. 2004, **35**(4), 203-207. DOI: 10.1002/mawe.200400735. ISSN 0933-5137.
Available at: http://doi.wiley.com/10.1002/mawe.200400735
[25] BOANINI, Elisa, Massimo GAZZANO, Carlo NERVI, Michele R. CHIEROTTI, Katia RUBINI, Roberto GOBETTO and Adriana BIGI. Strontium and Zinc Substitution in β-Tricalcium Phosphate: An X-ray Diffraction, Solid State NMR and ATR-FTIR Study. *Journal of Functional Biomaterials*. 2019, **10**(2), 109-115. DOI: 10.3390/jfb10020020. ISSN 2079-4983.
Available at: https://www.mdpi.com/2079-4983/10/2/20
[26] MARQUES, Catarina F., Fidel Hugo PERERA, Ana MAROTE, Sónia FERREIRA, Sandra I. VIEIRA, Susana OLHERO, Pedro MIRANDA and José M.F. FERREIRA. Biphasic calcium phosphate scaffolds fabricated by direct write assembly: Mechanical, anti-microbial and osteoblastic properties. *Journal of the European Ceramic Society*. 2017, **37**(1), 359-368. DOI: 10.1016/j.jeurceramsoc.2016.08.018. ISSN 09552219.
Available at: https://linkinghub.elsevier.com/retrieve/pii/S0955221916304526
[27] BERGMANN, Christian J. D., Jim C. E. ODEKERKEN, Tim J. M. WELTING, et al. Calcium Phosphate Based Three-Dimensional Cold Plotted Bone Scaffolds for Critical Size Bone Defects. *BioMed Research International*. 2014, **2014**(8), 1-10. DOI: 10.1155/2014/852610. ISSN 2314-6133. Available at: http://www.hindawi.com/journals/bmri/2014/852610/

[28] ELLIOTT, J. C. Structure and chemistry of the apatites and other calcium orthophosphates. New York: Elsevier, 1994. ISBN 04-448-1582-1.
[29] ZHOU, Ding, Chao QI, Yi-Xuan CHEN, Ying-Jie ZHU, Tuan-Wei SUN, Feng CHEN and Chang-Qing ZHANG. Comparative study of porous hydroxyapatite/chitosan and whitlockite/chitosan scaffolds for bone regeneration in calvarial defects. International Journal of Nanomedicine. 2017, 12(3), 2673-2687. DOI: 10.2147/IJN.S131251. ISSN 1178-2013. Available at:
https://www.dovepress.com/comparative-study-of-porous-hydroxyapatitechitosan-and-whitlockitechit-peer-reviewed-article-IJN
[30] ŠIMKOVÁ, Lenka, Nataliia Oleksandrivna GORODYLOVA and Petra ŠULCOVÁ. UNIVERZITA PARDUBICE. *Sborník příspěvků: 19. ročník konference o speciálních anorganických pigmentech a práškových materiálech KSAP-PM 2017*. 2017, 1-6. Application of Doped Hydroxyapatite as a Corrosion Inhibitor.
Available at: https://hdl.handle.net/10195/69814
[31] XIA, Zhiguo and Quanlin LIU. Progress in discovery and structural design of color conversion phosphors for LEDs. Progress in Materials Science. 2016, 84(1), 59-117. DOI: 10.1016/j.pmatsci.2016.09.007. ISSN 00796425.
Available at: https://linkinghub.elsevier.com/retrieve/pii/S0079642516300640
[32] KIM, Hwan D., Hae Lin JANG, Hyo-Yong AHN, et al. Biomimetic whitlockite inorganic nanoparticles-mediated in situ remodeling and rapid bone regeneration. Biomaterials. 2017, 112(1), 31-43. DOI: 10.1016/j.biomaterials.2016.10.009. ISSN 01429612.
Available at: https://linkinghub.elsevier.com/retrieve/pii/S0142961216305518
[33] JANG, Hae Lin, Guang Bin ZHENG, Jungha PARK, et al. In Vitro and In Vivo Evaluation of Whitlockite Biocompatibility: Comparative Study with Hydroxyapatite and β -tricalcium Phosphate. Advanced Healthcare Materials. 2016, 5(1), 128-136. DOI: 10.1002/adhm.201400824. ISSN 21922640.
Available at: http://doi.wiley.com/10.1002/adhm.201400824
[34] MANJUBALA, I., T. P. SASTRY a R. V. Suresh KUMAR. Bone In-growth Induced by Biphasic Calcium Phosphate Ceramic in Femoral Defect of Dogs. *Journal of Biomaterials Applications*. 2016, **19**(4), 341-360. DOI: 10.1177/0885328205048633. ISSN 0885-3282. Available at: http://journals.sagepub.com/doi/10.1177/0885328205048633
[35] ELIAZ, Noam a Noah METOKI. Calcium Phosphate Bioceramics: A Review of Their History, Structure, Properties, Coating Technologies and Biomedical Applications. *Materials*. 2017, **10**(4). DOI: 10.3390/ma10040334. ISSN 1996-1944. Available at: http://www.mdpi.com/1996-1944/10/4/334
[36] SUÁREZ, Sebastian, Leander REINERT a Frank MÜCKLICH. Carbon Nanotube (CNT)-Reinforced Metal Matrix Bulk Composites: Manufacturing and Evaluation. Diamond and

Carbon Composites and Nanocomposites. InTech, 2016, 2016-06-29. DOI: 10.5772/63886. ISBN 978-953-51-2453-5.
Available at:
http://www.intechopen.com/books/diamond-and-carbon-composites-and-nanocomposites/carbon-nanotube-cnt-reinforced-metal-matrix-bulk-composites-manufacturing-and-evaluation
[37] GALUSEK, D., P. ZNÁŠIK a J. MAJLING. The influence of cold isostatic pressing on compaction and properties of Mg-PSZ ceramics. Journal of Materials Science Letters. 1999, 18(16), 1347-1351. DOI: 10.1023/A:1006690500585. ISSN 02618028.
Available at: http://link.springer.com/10.1023/A:1006690500585
[38] AKIMOV, G. Ya. Cold isostatic pressing as a method for fabricating ceramic products with high physicomechanical properties. *Refractories and Industrial Ceramics*. 1998, **39**(7-8), 283-287. DOI: 10.1007/BF02765082. ISSN 1083-4877.
Available at: http://link.springer.com/10.1007/BF02765082
[39] RAMESH, S., P. CHRISTOPHER, C. Y. TAN a W. D. TENG. THE EFFECT OF COLD ISOSTATIC PRESSING ON THE SINTERABILITY OF SYNTHESIZED HA. Biomedical Engineering: Applications, Basis and Communications. 2012, 16(04), 199-204. DOI: 10.4015/S101623720400027X. ISSN 1016-2372.
Available at: https://www.worldscientific.com/doi/abs/10.4015/S101623720400027X
[40] TILLER, FRANK M. a CHUN-DAR TSAI. Theory of Filtration of Ceramics: I, Slip Casting. Journal of the American Ceramic Society. 1986, 69(12), 882-887. DOI: 10.1111/j.1151-2916.1986.tb07388.x. ISSN 0002-7820.
Available at: http://doi.wiley.com/10.1111/j.1151-2916.1986.tb07388.x
[41] BUCK, Gregory M. a Peter VASQUEZ. Ceramic slip casting technique. 1992. The United States of America. 5266525 US Patent. Date of patent: Nov. 30, 1993. Filled: Sep. 22, 1992.
[42] FUKASAWA, Takayuki, Motohide ANDO, Tatsuki OHJI a Shuzo KANZAKI. Synthesis of Porous Ceramics with Complex Pore Structure by Freeze-Dry Processing. *Journal of the American Ceramic Society*. 2001, **84**(1), 230-232. DOI: 10.1111/j.1151-2916.2001.tb00638.x. ISSN 00027820. Available at: http://doi.wiley.com/10.1111/j.1151-2916.2001.tb00638.x
[43] DEVILLE, Sylvain. Freeze-Casting of Porous Biomaterials: Structure, Properties and Opportunities. *Materials*. 2010, **3**(3), 1913-1927. DOI: 10.3390/ma3031913. ISSN 1996-1944.
Available at: http://www.mdpi.com/1996-1944/3/3/1913
[44] DEVILLE, S. Freeze-Casting of Porous Ceramics: A Review of Current Achievements and Issues. *Advanced Engineering Materials*. 2008, **10**(3), 155-169. DOI: 10.1002/adem.200700270. ISSN 14381656.
Available at: http://doi.wiley.com/10.1002/adem.200700270

[45] DEVILLE, Sylvain. Ice-templating, freeze casting: Beyond materials processing. *Journal of Materials Research*. 2013, **28**(17), 2202-2219. DOI: 10.1557/jmr.2013.105.
ISSN 0884-2914. Available at:
https://www.cambridge.org/core/product/identifier/S0884291413001052/type/journal_article
[46] DEVILLE, Sylvain, Sylvain MEILLE a Jordi SEUBA. A meta-analysis of the mechanical properties of ice-templated ceramics and metals. *Science and Technology of Advanced Materials*. 2016, **16**(4), 1-16. DOI: 10.1088/1468-6996/16/4/043501. ISSN 1468-6996. Available at: http://www.tandfonline.com/doi/full/10.1088/1468-6996/16/4/043501
[47] Kurapova, O. Y., Konakov, V. G., Golubev, S. N., Ushakov, V. M., & Archakov, I. Y. (2012). Cryochemical Methods For Manufacturing Nanosized Ceramics And Ceramic Precursor Powders With Low Agglomeration Degree: A Review. *Reviews on Advanced Materials Science*, *32*(2), 112-132.
[48] ARAKI, Kiyoshi a John W. HALLORAN. New Freeze-Casting Technique for Ceramics with Sublimable Vehicles. *Journal of the American Ceramic Society*. 2004, **87**(10), 1859-1863. DOI: 10.1111/j.1151-2916.2004.tb06331.x. ISSN 00027820.
Available at: http://doi.wiley.com/10.1111/j.1151-2916.2004.tb06331.x
[49] SOFIE, Stephen W. Fabrication of Functionally Graded and Aligned Porosity in Thin Ceramic Substrates With the Novel Freeze Tape-Casting Process. *Journal of the American Ceramic Society*. 2007, **90**(7), 2024-2031. DOI: 10.1111/j.1551-2916.2007.01720.x. ISSN 0002-7820. Available at: http://doi.wiley.com/10.1111/j.1551-2916.2007.01720.x
[50] ZHENG, Jumeng, Louis WINNUBST, VELIANTI, Shumin FANG a David SALAMON. Manipulation of Sintering Behavior by Initial Freeze Pressing an Aqueous Alumina Suspension. *Advanced Engineering Materials*. 2011, **13**(1-2), 77-81. DOI: 10.1002/adem.201000199. ISSN 14381656.
Available at: http://doi.wiley.com/10.1002/adem.201000199
[51] WEGST, Ulrike G. K., Matthew SCHECTER, Amalie E. DONIUS a Philipp M. HUNGER. Biomaterials by freeze casting. *Philosophical Transactions of the Royal Society A: Mathematical, Physical and Engineering Sciences*. 2010, **368**(1917), 2099-2121. DOI: 10.1098/rsta.2010.0014. ISSN 1364-503X.
Available at: https://royalsocietypublishing.org/doi/10.1098/rsta.2010.0014
[52] MUNCH, Etienne, Eduardo SAIZ, Antoni P. TOMSIA a Sylvain DEVILLE. Architectural Control of Freeze-Cast Ceramics Through Additives and Templating. *Journal of the American Ceramic Society*. 2009, **92**(7), 1534-1539. DOI: 10.1111/j.1551-2916.2009.03087.x. ISSN 00027820. Available at: http://doi.wiley.com/10.1111/j.1551-2916.2009.03087.x
[53] PORTER, Michael M., Joanna MCKITTRICK a Marc A. MEYERS. Biomimetic Materials by Freeze Casting. *JOM*. 2013, **65**(6), 720-727. DOI: 10.1007/s11837-013-0606-3. ISSN 1047-4838. Available at: http://link.springer.com/10.1007/s11837-013-0606-3

[54] DEVILLE, S. Freezing as a Path to Build Complex Composites. *Science*. 2006, **311**(5760), 515-518. DOI: 10.1126/science.1120937. ISSN 0036-8075.
Available at: https://www.sciencemag.org/lookup/doi/10.1126/science.1120937
[55] DEVILLE, Sylvain, Eric MAIRE, Audrey LASALLE, Agnès BOGNER, Catherine GAUTHIER, Jérôme LELOUP a Christian GUIZARD. In Situ X-Ray Radiography and Tomography Observations of the Solidification of Aqueous Alumina Particle Suspensions-Part I: Initial Instants. *Journal of the American Ceramic Society*. 2009, **92**(11), 2489-2496. DOI: 10.1111/j.1551-2916.2009.03163.x. ISSN 00027820.
Available at: http://doi.wiley.com/10.1111/j.1551-2916.2009.03163.
[56] ABDELWAHED, W, G DEGOBERT, S STAINMESSE a H FESSI. Freeze-drying of nanoparticles: Formulation, process and storage considerations. *Advanced Drug Delivery Reviews*. 2006, **58**(15), 1688-1713. DOI: 10.1016/j.addr.2006.09.017. ISSN 0169409X.
Available at: https://linkinghub.elsevier.com/retrieve/pii/S0169409X06001840
[57] FRANKS, Felix. Freeze-drying of bioproducts: putting principles into practice. *European Journal of Pharmaceutics and Biopharmaceutics*. 1998, **45**(3), 221-229. DOI: 10.1016/S0939-6411(98)00004-6. ISSN 09396411.
Available at: https://linkinghub.elsevier.com/retrieve/pii/S0939641198000046
[58] DEVILLE, Sylvain, Eduardo SAIZ and Antoni P. TOMSIA. Freeze casting of hydroxyapatite scaffolds for bone tissue engineering. *Biomaterials*. 2006, **27**(32), 5480-5489. DOI: 10.1016/j.biomaterials.2006.06.028. ISSN 01429612.
Available at: https://linkinghub.elsevier.com/retrieve/pii/S0142961206005801
[59] LI, W L, K LU a J Y WALZ. Freeze casting of porous materials: review of critical factors in microstructure evolution. *International Materials Reviews*. 2013, **57**(1), 37-60. DOI: 10.1179/1743280411Y.0000000011. ISSN 0950-6608.
Available at: http://www.tandfonline.com/doi/full/10.1179/1743280411Y.0000000011
[60] ZUO, Kai Hui, Yu-Ping ZENG a Dongliang JIANG. Effect of polyvinyl alcohol additive on the pore structure and morphology of the freeze-cast hydroxyapatite ceramics. *Materials Science and Engineering: C*. 2010, **30**(2), 283-287. DOI: 10.1016/j.msec.2009.11.003. ISSN 09284931.
Available at: https://linkinghub.elsevier.com/retrieve/pii/S0928493109002835
[61] TOTH, Jeffrey M., Walter M. HIRTHE, William G. HUBBARD, William A. BRANTLEY a Kenneth L. LYNCH. Determination of the ratio of HA/TCP mixtures by x-ray diffraction. *Journal of Applied Biomaterials*. 1991, **2**(1), 37-40. DOI: 10.1002/jab.770020106. ISSN 10454861.
Available at: http://doi.wiley.com/10.1002/jab.770020106
[62] EN 623-2. Advanced technical ceramics. Monolithic ceramics. General and textural properties. Determination of density and porosity. British standard, 1993.

[63] ZYMAN, Z., J. WENG, X. LIU, X. LI a X. ZHANG. Phase and structural changes in hydroxyapatite coatings under heat treatment. Biomaterials. 1994, 15(2), 151-155. DOI: 10.1016/0142-9612(94)90265-8. ISSN 01429612.
Available at: https://linkinghub.elsevier.com/retrieve/pii/0142961294902658
[64] CHU, Kuo-Tien, Shih-Fu OU, Shyuan-Yow CHEN, Shi-Yung CHIOU, Hsin-Hua CHOU a Keng-Liang OU. Research of phase transformation induced biodegradable properties on hydroxyapatite and tricalcium phosphate based bioceramic. *Ceramics International*. 2013, **39**(2), 1455-1462. DOI: 10.1016/j.ceramint.2012.07.089. ISSN 02728842. Available at: https://linkinghub.elsevier.com/retrieve/pii/S0272884212007237
[65] OU, Shih-Fu, Shi-Yung CHIOU a Keng-Liang OU. Phase transformation on hydroxyapatite decomposition. *Ceramics International*. 2013, **39**(4), 3809-3816. DOI: 10.1016/j.ceramint.2012.10.221. ISSN 02728842.
Available at: https://linkinghub.elsevier.com/retrieve/pii/S0272884212011844
[66] MURALITHRAN, G a S RAMESH. The effects of sintering temperature on the properties of hydroxyapatite. *Ceramics International*. 2000, **26**(2), 221-230. DOI: 10.1016/S0272-8842(99)00046-2. ISSN 02728842.
Available at: https://linkinghub.elsevier.com/retrieve/pii/S0272884299000462
[67] CUSCÓ, R., F. GUITIÁN, S.de AZA a L. ARTÚS. Differentiation between hydroxyapatite and β-tricalcium phosphate by means of μ-Raman spectroscopy. *Journal of the European Ceramic Society*. 1998, **18**(9), 1301-1305. DOI: 10.1016/S0955-2219(98)00057-0.
ISSN 09552219. Available at: https://linkinghub.elsevier.com/retrieve/pii/S0955221998000570
[68] DE AZA, P. N., C. SANTOS, A. PAZO, S. DE AZA, R. CUSCÓ a L. ARTÚS. Vibrational Properties of Calcium Phosphate Compounds. 1. Raman Spectrum of β-Tricalcium Phosphate. *Chemistry of Materials*. 1997, **9**(4), 912-915. DOI: 10.1021/cm960425d.
ISSN 0897-4756. Available at: https://pubs.acs.org/doi/10.1021/cm960425d
[69] DE AZA, P. N., F. GUITIÁN, C. SANTOS, S. DE AZA, R. CUSCÓ a L. ARTÚS. Vibrational Properties of Calcium Phosphate Compounds. 2. Comparison between Hydroxyapatite and β-Tricalcium Phosphate. *Chemistry of Materials*. 1997, **9**(4), 916-922. DOI: 10.1021/cm9604266. ISSN 0897-4756.
Available at: https://pubs.acs.org/doi/10.1021/cm9604266

9 LIST OF ABBREVIATIONS

CaP	Calcium phosphate
HA	Hydroxyapatite
TCP	Tricalcium phosphate
WH	Whitlockite
DCPA	Dicalcium phosphate
TTCP	Tetracalcium phosphate
CIP	Cold isostatic pressing
SEM	Scanning electron microscopy
XRD	X-ray diffractometry